

## Theory of exciton pair states and their nonlinear optical properties in semiconductor quantum dots

Selvakumar V. Nair\* and Toshihide Takagahara

*NTT Basic Research Laboratories, 3-1 Morinosato Wakamiya, Atsugi-shi, 243 Japan*

(Received 26 September 1996)

The exciton and two-exciton states in semiconductor quantum dots much larger in size than the exciton Bohr radius are investigated, and the energies and oscillator strengths of several exciton and biexciton states are calculated. The presence of weakly correlated exciton-pair states are identified and these have a large oscillator strength increasing proportional to the volume of the quantum dot. These states are shown to play a crucial role in determining the nonlinear optical response of large quantum dots. The weakly correlated exciton-pair states are found to cause a cancellation effect in the third-order nonlinear optical susceptibility at the exciton resonance, providing a consistent understanding of the experimentally observed saturation of the mesoscopic enhancement of the excitonic optical nonlinearity. The excited-state absorption in quantum dots is also studied and the excitation of the weakly correlated exciton-pair states is found to dominate the spectrum. The spectral features in the pump-probe spectroscopy are predicted in detail. The biexciton binding energy and oscillator strength are obtained in good agreement with experimental results on CuCl quantum dots. Also, the good correspondence of the excited-state absorption spectra between the theory and experiments provides convincing evidence for the presence of the weakly correlated exciton-pair states. [S0163-1829(97)04008-3]

### I. INTRODUCTION

Optical properties of three-dimensionally confined electrons and holes in semiconductor microcrystals (quantum dots) have been extensively studied in recent years.<sup>1</sup> This work has been fueled in part by interest in the fundamental physics of finite systems as well as by their potential as efficient nonlinear optical and laser materials.<sup>2-12</sup> The spatial confinement of electrons and holes leads to a discrete energy level structure with possibly sharp absorption lines as in atoms. The concentration of the oscillator strength into well-defined energies makes quantum dots (QD's) very attractive for electro-optic and nonlinear optical applications.

In addition to the spatial confinement, the Coulomb interaction between the excited electrons and holes also plays an important role in determining the excitation spectra of QD's. This is especially true in most of the currently studied crystallites of II-VI and I-VII semiconductors like CdS, CdSe, CuCl, etc., owing to the large exciton binding energy in these materials. The formation of excitons and biexcitons in dots of radius ( $R$ ) larger than several times the exciton Bohr radius ( $a_{\text{ex}}$ ) leads to a strong optical response at the exciton resonance. In fact, in this weak confinement regime ( $R \gg a_{\text{ex}}$ ),<sup>13</sup> the exciton oscillator strength is proportional to the volume of the quantum dot. Consequent superradiant decay of the exciton has been experimentally observed<sup>14,15</sup> with the lifetime decreasing inversely as the volume of the QD. The mesoscopic enhancement of the exciton oscillator strength would lead to, for example, a nonlinear optical susceptibility increasing with the size of the QD.<sup>16</sup> The nonlinear response is, however, determined not only by the exciton states but also by multiple-exciton states and especially by the biexcitonic excitations. Many recent experiments on CuCl QD's in the weak confinement regime have revealed

distinctly non-bulk-like features including enhanced nonlinear optical susceptibility with an intriguing size dependence,<sup>10</sup> very large gain for biexcitonic lasing,<sup>9</sup> and a blueshift of the excitonic absorption under a strong pump beam.<sup>17</sup> These observations indicate the significance of the interplay of excitonic and biexcitonic states.

Theoretically, considerable progress has been achieved in the description of the single-particle electronic structure providing a satisfactory framework for describing the optical response of QD's of a radius comparable to or smaller than  $a_{\text{ex}}$ .<sup>18-22</sup> In larger crystallites, reliable theoretical calculations of the excitonic states exist.<sup>23-27</sup> However, biexciton calculations<sup>3,28</sup> have been restricted to QD's whose radius is smaller than a few times  $a_{\text{ex}}$ , due to the numerical complexity of the problem when  $R \gg a_{\text{ex}}$ . There has also been a study of the biexciton states in the asymptotic limit of  $R \rightarrow \infty$  using a simplified exciton-exciton interaction.<sup>29</sup>

Motivated by these considerations, we study the size dependence of the biexcitonic states and of the nonlinear optical response of semiconductor QD's of radii up to  $10a_{\text{ex}}$  using an approach based on an exciton-exciton product state basis. We obtain the biexciton binding energy and oscillator strengths in reasonable agreement with experimental results. Most importantly, we identify the presence of a weakly correlated exciton pair state with a large oscillator strength, which provides important insights into various features of the experimental observations mentioned above.<sup>9,10,17</sup> We calculate the third-order nonlinear optical susceptibility at the exciton resonance and clarify the physics of the observed saturation<sup>10</sup> of the mesoscopic enhancement which has so far eluded a satisfactory explanation. We also study the excited-state absorption from the exciton ground state. From the comparison between the theory and experiments, we obtain a convincing evidence for the presence of the weakly corre-

lated exciton pair states. Some of these results have been briefly reported in a previous publication.<sup>30</sup>

The paper is organized as follows. In Sec. II, we present the theoretical details of the calculation of the exciton and biexciton energy levels and dipole moments within the effective mass approximation (EMA) including the electron-hole exchange interaction. In Sec. III we discuss the calculated energy levels and oscillator strengths of the exciton and biexciton states. In Sec. IV we present the nonlinear optical response at the exciton resonance and clarify the physics of the intriguing size dependence of the optical nonlinearity. Furthermore, we discuss the excited-state absorption from the exciton ground state. Finally, in Sec. V we summarize our results.

## II. THEORETICAL FORMULATION

We investigate semiconductor quantum dots of a radius ( $R$ ) larger than the Bohr radius of the exciton ( $a_{\text{ex}}$ ) in the bulk material. In this size range, the electronic excitations close to the band gap may be described using the EMA.

$$\left[ -\frac{\hbar^2}{2m_e}\nabla_e^2 - \frac{\hbar^2}{2m_h}\nabla_h^2 - \frac{e^2}{\epsilon r_{\text{eh}}} + V \right] \phi(\mathbf{r}_e, \mathbf{r}_h) = (E - E_g) \phi(\mathbf{r}_e, \mathbf{r}_h), \quad (1)$$

where  $m_e$  ( $m_h$ ) and  $\mathbf{r}_e$  ( $\mathbf{r}_h$ ), respectively, denote the effective mass and the position vector of the electron (hole),  $r_{\text{eh}} = |\mathbf{r}_e - \mathbf{r}_h|$ ,  $\epsilon$  is the bulk dielectric constant, and  $E_g$  is the bulk band gap. The confining potential  $V$  is zero inside the QD of radius  $R$ , and infinite outside, with the corresponding boundary condition

$$\phi(\mathbf{r}_e, \mathbf{r}_h) = 0 \quad \text{for } r_e \text{ or } r_h \geq R. \quad (2)$$

Here we have neglected the image charge effects arising from the dielectric mismatch between the QD and the host material. This is expected to be small in the large size range of interest to us.

For  $R$  smaller than a few times  $a_{\text{ex}}$ , the exciton states can be calculated by expanding into single-particle product states as has been successfully demonstrated earlier.<sup>24,28</sup> However, when  $R$  is larger than several times  $a_{\text{ex}}$ , the case that we are interested in, the electron-hole Coulomb interaction is large compared to the confinement kinetic energy and consequently a single-particle product state approach is numerically prohibitive. The exciton ground state in this so-called weak confinement regime has been calculated by several authors using the variational approach.<sup>23-26</sup> Several excited states also have been calculated using a basis set of electron-hole correlated functions involving polynomials and exponentials.<sup>26</sup> We use this formulation to calculate the excitonic states.

Owing to the spherical symmetry of the problem, the exciton envelope function can be labeled by the envelope an-

Since most experimental samples consist of a dilute collection of nearly spherical crystallites, we study a single crystallite of spherical shape. The spherical symmetry greatly reduces the numerical complexity of the problem.

The success of our calculation is based on avoiding the use of a single-particle product basis for the calculation of the exciton and biexciton states, as this is numerically prohibitive, especially for the four-particle biexcitonic states. Instead, we use an exciton-exciton product basis for the biexciton calculation. Working within the EMA, we first calculate a number of the low energy exciton states using a correlated basis set used earlier by Kayanuma<sup>26</sup> for the  $L=0$  excitons, which we extend to  $L>0$  states, where  $L$  is the angular momentum of the exciton envelope function.

### A. Exciton states

Within the EMA, the wave function  $\phi(\mathbf{r}_e, \mathbf{r}_h)$ , for a single electron-hole pair is determined by the effective Schrödinger equation,

gular momentum  $L$ . We expand the  $L=0$  exciton envelope function into a set of nonorthogonal basis functions,<sup>26</sup>

$$\begin{aligned} \phi_0(\mathbf{r}_e, \mathbf{r}_h) = & \sum_{l=0}^{l_{\text{max}}} \sum_{m=0}^{m_{\text{max}}} \sum_{n=0}^{n_{\text{max}}} c_{lmn} w_m(r_e) w_n(r_h) r_{\text{eh}}^l \\ & \times \exp(-r_{\text{eh}}/a_{\text{ex}}) \end{aligned} \quad (3a)$$

with

$$w_m(r) = \prod_{k=1}^m \left[ r^2 - \left[ \frac{k}{m} R \right]^2 \right], \quad (3b)$$

which explicitly satisfies the boundary condition given by Eq. (2). The coefficients  $c_{lmn}$  are then determined by a generalized eigenvalue equation which may be solved by standard numerical techniques. Truncating the expansion Eq. (3a), with  $m_{\text{max}} = n_{\text{max}} = 3$  and  $l_{\text{max}} = 2$ , several exciton energy levels are obtained with a high accuracy.<sup>26</sup>

Although only the  $L=0$  excitons are optically excited in a direct gap semiconductor, the  $L>0$  states also need to be calculated to construct a reasonably complete exciton-exciton product state basis. A straightforward generalization of the above approach leads to the expansion,

$$\phi_{LM}(\mathbf{r}_e, \mathbf{r}_h) = \sum_{l_1=0}^{l_{\max}} \sum_{l_2=|l_1-L|}^{l_1+L} F_{l_1 l_2}(r_e, r_h) \sum_{m=-l_1}^{l_1} C_{m, M-m, M}^{l_1, l_2, L} Y_{l_1 m}(\Omega_e) Y_{l_2, M-m}(\Omega_h), \quad (4)$$

where  $C_{m, M-m, M}^{l_1, l_2, L}$ 's denote the Clebsch-Gordan coefficients and  $Y_{lm}$ 's are the spherical harmonics. However, the use of such an expansion is computationally intensive because of the need to keep a large number of terms in the sum over the angular functions.

Instead, we extend Kayanuma's approach to  $L=1$  states by noting that, for two particles, any odd-parity,  $L=1$  state can be expressed in the form (see Appendix A)

$$\phi_{1M}^i(\mathbf{r}_e, \mathbf{r}_h) = f_e^i(r_e, r_h, r_{\text{ch}}) Y_{1M}(\Omega_e) + f_h^i(r_e, r_h, r_{\text{ch}}) Y_{1M}(\Omega_h), \quad (5)$$

where  $i$  denotes the radial quantum number. This allows us to describe the  $L=1$  states in terms of two functions,  $f_e$  and  $f_h$ , of the Hylleraas coordinates, and the same basis set used for the  $L=0$  case can be used to expand  $f_e$  and  $f_h$ .

For  $L>1$  states, no such simple form appears to exist. In the present calculation we consider only the  $L \leq 2$  states, and any  $L=2$ , even parity state can be written as (see Appendix A)

$$\begin{aligned} \phi_{2M}^i(\mathbf{r}_e, \mathbf{r}_h) &= g_e^i(r_e, r_h, r_{\text{ch}}) Y_{2M}(\Omega_e) \\ &+ g_h^i(r_e, r_h, r_{\text{ch}}) Y_{2M}(\Omega_h) + \sum_{l \geq 4}^{\infty} \tilde{g}_l^i(r_e, r_h) \\ &\times \sum_m C_{m, M-m, M}^{l, l, 2} Y_{lm}(\Omega_e) Y_{l, M-m}(\Omega_h). \end{aligned} \quad (6)$$

We note that the sum in the third term in Eq. (6) starts at  $l=4$  and so the relatively slowly varying envelope of the low energy states would be well described by the first two terms. This expectation is borne out by our numerical results and thus, to a good approximation, the  $L=2$  exciton states also may be written in a form identical to the  $L=1$  states.

Although a general two-particle state of angular momentum  $L$  can have either parity, we consider only those states with parity  $(-1)^L$  as all the low energy states in relatively large QD's will have this parity. This becomes apparent by noting that in the size range being considered, the exciton envelope function is approximately given by the product of the bulk exciton wave function for the relative coordinate and a particle-in-a-sphere wave function for the confinement of the center of mass motion.<sup>13</sup> As the first excited state of a hydrogenic system has a binding energy of only 1/4 times that of the ground state, it follows that all the low energy states will involve the  $s$ -like relative coordinate wave function so that the angular momentum is determined by that of the center of mass motion alone. Such states will have a parity  $(-1)^L$ .

### B. Biexciton states

The EMA Hamiltonian for two electrons and two holes is given by

$$\begin{aligned} H_{XX} &= -\frac{\hbar^2}{2m_e} (\nabla_{e_1}^2 + \nabla_{e_2}^2) - \frac{\hbar^2}{2m_h} (\nabla_{h_1}^2 + \nabla_{h_2}^2) - \frac{e^2}{\epsilon |\mathbf{r}_{e_1} - \mathbf{r}_{h_1}|} \\ &- \frac{e^2}{\epsilon |\mathbf{r}_{e_1} - \mathbf{r}_{h_2}|} - \frac{e^2}{\epsilon |\mathbf{r}_{e_2} - \mathbf{r}_{h_1}|} - \frac{e^2}{\epsilon |\mathbf{r}_{e_2} - \mathbf{r}_{h_2}|} \\ &+ \frac{e^2}{\epsilon |\mathbf{r}_{e_1} - \mathbf{r}_{e_2}|} + \frac{e^2}{\epsilon |\mathbf{r}_{h_1} - \mathbf{r}_{h_2}|}. \end{aligned} \quad (7)$$

Again we neglect the image charge effects as in the case for the exciton states. As all the optically excited states have a vanishing angular momentum ( $L=0$ ) for the envelope function, we consider only such biexciton states. Biexciton states  $\Phi(\mathbf{r}_{e_1}, \mathbf{r}_{h_1}, \mathbf{r}_{e_2}, \mathbf{r}_{h_2})$  with  $L=0$  may be expanded into the exciton-exciton product states:

$$\Phi(\mathbf{r}_{e_1}, \mathbf{r}_{h_1}, \mathbf{r}_{e_2}, \mathbf{r}_{h_2}) = \sum_{ijL} C_{ijL} G_{XX}^{ijL} + \tilde{C}_{ijL} \tilde{G}_{XX}^{ijL} \quad (8a)$$

with  $G$  and  $\tilde{G}$  given by

$$G_{XX}^{ijL} = \sum_{M=-L}^L \phi_{LM}^i(\mathbf{r}_{e_1}, \mathbf{r}_{h_1}) \phi_{LM}^{j*}(\mathbf{r}_{e_2}, \mathbf{r}_{h_2}), \quad (8b)$$

$$\tilde{G}_{XX}^{ijL} = \sum_{M=-L}^L \phi_{LM}^i(\mathbf{r}_{e_1}, \mathbf{r}_{h_2}) \phi_{LM}^{j*}(\mathbf{r}_{e_2}, \mathbf{r}_{h_1}). \quad (8c)$$

Here  $i, j$  denote the radial quantum numbers of the exciton eigenstates. Since the Hamiltonian is invariant under exchange of the electron or hole coordinates, the biexciton wave function can be labeled by symmetry under permutations of the coordinates. We denote states that are symmetric (antisymmetric) under electron exchange by a superscript  $+$  ( $-$ ). A second superscript of  $\pm$  is used to denote the symmetry under hole exchange. Thus,  $\Phi^{\pm\pm}$  denotes states with  $C_{ijL} = C_{jiL} = \pm \tilde{C}_{ijL}$ , while  $\Phi^{\mp\pm}$  denotes states with  $C_{ijL} = -C_{jiL} = \pm \tilde{C}_{ijL}$ . For the largest QD, we use four  $L=0$ , three  $L=1$  and two  $L=2$ , states giving a total of 58 product states forming a nonorthogonal basis.

### C. Electron-hole exchange interaction

Although the electron-hole exchange interaction has been extensively discussed in the past,<sup>31</sup> we reformulate the problem in a form suitable for applying to QD's within the effective mass approximation. The exciton and the biexciton Hamiltonian including the electron-hole exchange interaction within the EMA are derived in Appendix B. For the exciton we have

$$\left[ -\frac{\hbar^2}{2m_e}\nabla_e^2 - \frac{\hbar^2}{2m_h}\nabla_h^2 - \frac{e^2}{\epsilon r_{eh}} + \delta_{I,1}\Delta E_{\text{exch}}^0 \pi a_{\text{ex}}^3 \delta(\mathbf{r}_e - \mathbf{r}_h) \right] \phi(\mathbf{r}_e, \mathbf{r}_h) = (E - E_g) \phi(\mathbf{r}_e, \mathbf{r}_h), \quad (9)$$

where  $\Delta E_{\text{exch}}^0$  is the bulk exciton exchange splitting energy and  $I$  is the sum of the electron and hole Bloch function angular momenta. For the case of the  $\Gamma_6$  conduction band and the  $\Gamma_7$  valence band of cubic materials that we consider (see Appendix B), the  $I=1$  state is threefold degenerate and is a mixture of spin-singlet and spin-triplet electron-hole pair states. The  $I=0$  state which has no exchange contribution to the energy is purely spin triplet.<sup>31</sup>

At this point, it is useful to review some details of the symmetry of the electron and hole Bloch functions and that of the exciton. As we consider spherical QD's and use spherical band dispersion for the EMA, the band edge Bloch function of  $\Gamma_6$  symmetry transforms like an  $l=0, s=1/2$  orbital, while the  $\Gamma_7$  Bloch function transforms like an  $l=1, s=1/2, l+s=1/2$  orbital.<sup>32</sup> The four states of exciton that may be formed from these twofold degenerate electron and hole states split into a nondegenerate state of  $\Gamma_2$  symmetry and a threefold degenerate state of  $\Gamma_5$  symmetry. In the present case, these states may also be labeled by their total Bloch function angular momentum,  $I=0$  and 1, respectively. The corresponding products of the electron and hole Bloch functions are

$$\psi_{00} = \frac{1}{\sqrt{2}}(u_{c,1/2}u_{v,1/2}^* + u_{c,-1/2}u_{v,-1/2}^*), \quad (10a)$$

$$\psi_{10} = \frac{1}{\sqrt{2}}(u_{c,1/2}u_{v,1/2}^* - u_{c,-1/2}u_{v,-1/2}^*), \quad (10b)$$

$$\psi_{11} = -u_{c,1/2}u_{v,-1/2}^*, \quad (10c)$$

and

$$\psi_{1,-1} = u_{c,-1/2}u_{v,1/2}^*, \quad (10d)$$

where  $u_{c(v)}$ 's are the conduction (valence) band Bloch functions defined in Appendix B. It is the  $I=1$  exciton state that is optically excited as it contains the spin-singlet component. As all the optically excited states have a zero angular momentum ( $L$ ) for the envelope function, for such states  $I$  also equals the total angular momentum.

Equation (9) for the exciton including the electron-hole exchange interaction can be solved by expanding the exciton

wave function as described in Sec. II A. The exchange energy can, however, be obtained to a very good approximation within the first-order perturbation theory as

$$\Delta E_{\text{exch}} = \Delta E_{\text{exch}}^0 \pi a_{\text{ex}}^3 \int |\phi(\mathbf{r}, \mathbf{r})|^2 d^3r \quad (11)$$

for the  $I=1$  states and zero otherwise. Here,  $\phi(\mathbf{r}_e, \mathbf{r}_h)$  is the exciton envelope function calculated without including the exchange interaction. The wave function of the exciton is then given by the envelope function  $\phi$  times the Bloch function product  $\psi_{I_z}$  given by Eq. (10).

Now we consider the biexciton states. From  $I=0$  and  $I=1$  exciton states, we may generate biexciton states with the Bloch function angular momentum  $J=0, 1$ , or 2:

$$0 \otimes 0 = 0 \quad \text{or} \quad \Gamma_2 \otimes \Gamma_2 = \Gamma_1,$$

$$1 \otimes 0 = 1 \quad \text{or} \quad \Gamma_5 \otimes \Gamma_2 = \Gamma_4,$$

$$1 \otimes 1 = 0 \oplus 1 \oplus 2 \quad \text{or} \quad \Gamma_5 \otimes \Gamma_5 = \Gamma_1 \oplus \Gamma_4 \oplus (\Gamma_3 \oplus \Gamma_5).$$

Thus an  $I=0$  exciton pair will get mixed with an  $I=1$  pair to give  $J=0$  biexciton states, while  $I=1$  pairs will form  $J=2$  biexcitons and a pair made up of  $I=0$  and  $I=1$  excitons will mix with an  $I=1$  pair to give  $J=1$  biexcitons.

For those biexciton states with the envelope function angular momentum  $L=0$ , the case that we consider, the Bloch function angular momentum  $J$  completely determines the symmetry of the biexciton wave functions. However, the requirement of the antisymmetry of the wave function under the electron-electron or the hole-hole interchange puts some restrictions on the form of the envelope functions. As discussed in Sec. II B, we can have four kinds of exciton-exciton product states:  $\Phi^{++}$ ,  $\Phi^{--}$ ,  $\Phi^{+-}$ , and  $\Phi^{-+}$ . The  $J=0$  biexciton state may be written as

$$\Psi_{00} = \Phi_0^{++} \chi_{00}^{00} + \Phi_0^{--} \chi_{00}^{11}, \quad (12)$$

where  $\chi_{JJ_z}^{ss'}$  is the product of two-electron and two-hole Bloch function products with the total electron spin equal to  $s$  and the total hole angular momentum equal to  $s'$ , and  $J=s+s', s+s'-1, \dots, |s-s'|$ . Then, the EMA equation satisfied by  $\Phi_0^{++}$  and  $\Phi_0^{--}$  is (see Appendix B)

$$(H_{XX} - E)\Phi_0^{++} + \pi a_{\text{ex}}^3 \Delta E_{\text{exch}}^0 \left( \frac{3}{4}(\delta_1 + \delta_2 + \delta_3 + \delta_4)\Phi_0^{++} - \frac{\sqrt{3}}{4}(\delta_1 + \delta_2 - \delta_3 - \delta_4)\Phi_0^{--} \right) = 0, \quad (13a)$$

$$(H_{XX} - E)\Phi_0^{--} + \pi a_{\text{ex}}^3 \Delta E_{\text{exch}}^0 \left( \frac{-\sqrt{3}}{4}(\delta_1 + \delta_2 - \delta_3 - \delta_4)\Phi_0^{++} + \frac{1}{4}(\delta_1 + \delta_2 + \delta_3 + \delta_4)\Phi_0^{--} \right) = 0, \quad (13b)$$

where  $H_{XX}$  is the Hamiltonian given by Eq. (7),  $\delta_1 = \delta(\mathbf{r}_{e_1} - \mathbf{r}_{h_1})$ ,  $\delta_2 = \delta(\mathbf{r}_{e_2} - \mathbf{r}_{h_2})$ ,  $\delta_3 = \delta(\mathbf{r}_{e_1} - \mathbf{r}_{h_2})$ , and  $\delta_4 = \delta(\mathbf{r}_{e_2} - \mathbf{r}_{h_1})$ .

The  $J=1$  biexciton state with  $J_z=M$ , may be written as

$$\Psi_{1M} = \Phi_1^{--} \chi_{1M}^{11} + \Phi_1^{+-} \chi_{1M}^{01} + \Phi_1^{-+} \chi_{1M}^{10} \quad (14)$$

and the corresponding EMA equation is found to be

$$(H_{XX} - E) \Phi_1^{--} + \pi a_{\text{ex}}^3 \Delta E_{\text{exch}}^0 \left( \frac{1}{2} (\delta_1 + \delta_2 + \delta_3 + \delta_4) \Phi_1^{--} - \frac{1}{2\sqrt{2}} (\delta_1 + \delta_2 - \delta_3 - \delta_4) \Phi_1^{+-} - \frac{1}{2\sqrt{2}} (\delta_1 - \delta_2 + \delta_3 - \delta_4) \Phi_1^{-+} \right) = 0, \quad (15a)$$

$$(H_{XX} - E) \Phi_1^{+-} + \pi a_{\text{ex}}^3 \Delta E_{\text{exch}}^0 \left( -\frac{1}{2\sqrt{2}} (\delta_1 + \delta_2 - \delta_3 - \delta_4) \Phi_1^{--} + \frac{3}{4} (\delta_1 + \delta_2 + \delta_3 + \delta_4) \Phi_1^{+-} + \frac{1}{2} (\delta_1 - \delta_2 - \delta_3 + \delta_4) \Phi_1^{-+} \right) = 0, \quad (15b)$$

and

$$(H_{XX} - E) \Phi_1^{-+} + \pi a_{\text{ex}}^3 \Delta E_{\text{exch}}^0 \left( -\frac{1}{2\sqrt{2}} (\delta_1 - \delta_2 + \delta_3 - \delta_4) \Phi_1^{--} + \frac{1}{2} (\delta_1 - \delta_2 - \delta_3 + \delta_4) \Phi_1^{+-} + \frac{3}{4} (\delta_1 + \delta_2 + \delta_3 + \delta_4) \Phi_1^{-+} \right) = 0. \quad (15c)$$

The  $J=2$ ,  $J_z=M$  biexciton state has the form

$$\Psi_{2M} = \Phi_2^{--} \chi_{2M}^{11} \quad (16)$$

and  $\Phi_2^{--}$  satisfy

$$(H_{XX} - E) \Phi_2^{--} + \pi a_{\text{ex}}^3 \Delta E_{\text{exch}}^0 (\delta_1 + \delta_2 + \delta_3 + \delta_4) \Phi_2^{--} = 0. \quad (17)$$

Equations (13), (15), and (17) may be solved by expanding the functions  $\Phi$ 's into exciton-exciton product states as in the case without the exchange interaction described earlier.

#### D. Transition dipole moments

Now we calculate the transition dipole moments for excitation of the exciton states and the biexciton states. We consider only the interband transitions between the  $\Gamma_7$  valence band and the  $\Gamma_6$  conduction band. Then the polarization operator, in the second quantized site representation, is given by

$$P_z^+ = \mu_{\text{cv}} \sum_{\sigma} \int \hat{\psi}_{c\sigma}^{\dagger}(\mathbf{r}) \hat{\psi}_{v,-\sigma}^{\dagger}(\mathbf{r}) d^3r, \quad (18)$$

where  $\mu_{\text{cv}}$  is the interband transition dipole moment and the light polarization is assumed to be along the  $z$  axis. In terms of the conduction and valence band edge Bloch functions given by Eq. (B4),  $\mu_{\text{cv}} = -ie/(\sqrt{3}\Omega_{\text{cell}}) \int \zeta_z(\mathbf{r}) z \zeta_0(\mathbf{r}) d^3r$ , where the integral is over a unit cell of volume  $\Omega_{\text{cell}}$ . In this case, only the  $I=1$  exciton with  $I_z=0$  is excited from the ground state. Using the exciton state for  $I=1$ ,  $I_z=0$  given by

$$|X\rangle_{10} = \frac{1}{\sqrt{2}} \sum_{\sigma} \int d^3r_e d^3r_h \phi(\mathbf{r}_e, \mathbf{r}_h) \hat{\psi}_{c\sigma}^{\dagger}(\mathbf{r}_e) \hat{\psi}_{v,-\sigma}^{\dagger}(\mathbf{r}_h) |0\rangle, \quad (19)$$

we obtain the corresponding dipole moment to be

$$\mu_{10}^X = {}_{10}\langle X | P_z^+ | 0 \rangle = \sqrt{2} \mu_{\text{cv}} \int \phi(\mathbf{r}, \mathbf{r}) d^3r. \quad (20)$$

Now we consider the exciton to biexciton transitions. Again taking the light polarization to be along the  $z$  axis, only transitions which conserve the  $z$  component of the angular momentum are allowed. In addition, transitions that would cause the total spin to change are forbidden. These selection rules lead to the following restrictions: the  $J=0$  biexciton can be excited only from the  $I=1$ ,  $I_z=0$  exciton states, while the  $J=1$  biexciton states are excited from the  $I=0$  (if  $J_z=0$ ) and  $I=1$ ,  $I_z=J_z$  (if  $J_z \neq 0$ ) exciton states and the  $J=2$  biexciton states are excited only from the  $I=1$ ,  $I_z=J_z$  exciton states.

Using the second quantized form of the  $J=0$  biexciton state  $|XX\rangle_{00}$  corresponding to the wave function given by Eq. (12), we obtain the dipole moment for its excitation from  $|X\rangle_{10}$  to be

$$\mu_{00}^{XX} = {}_{00}\langle XX | P_z^+ | X \rangle_{10} = \sqrt{2} \mu_{\text{cv}} \int \left( \Phi_0^{++}(\mathbf{r}_e, \mathbf{r}_h, \mathbf{r}, \mathbf{r}) - \sqrt{\frac{1}{3}} \Phi_0^{--}(\mathbf{r}_e, \mathbf{r}_h, \mathbf{r}, \mathbf{r}) \right) \phi(\mathbf{r}_e, \mathbf{r}_h) d^3r_e d^3r_h d^3r. \quad (21)$$

In general, we may write the biexciton state of Bloch function angular momentum  $J$  and its  $z$  component  $M$  in a concise notation [cf. Eqs. (12), (14), and (16)]:

$$|XX\rangle_{JM} = a_J^{++} \Phi_J^{++} |\chi\rangle_{JM}^{00} + a_J^{--} \Phi_J^{--} |\chi\rangle_{JM}^{11} + a_J^{+-} \Phi_J^{+-} |\chi\rangle_{JM}^{01} + a_J^{-+} \Phi_J^{-+} |\chi\rangle_{JM}^{10}, \quad (22)$$

where  $a_J^{pp'} = 1$  if  $J=0$ ,  $p=p'$  or  $J=1$ ,  $p \neq p'$  or  $J=1$  or  $2$ ,  $p=p' = -$  and vanishes otherwise. Then the transition dipole moment from the exciton state  $|\chi\rangle_{IM}$  to the biexciton state  $|XX\rangle_{JM}$  may be expressed as

$$J_M \langle XX | P_z^+ | \chi \rangle_{IM} = \sqrt{2} \mu_{cv} \sum_{pp'} a_J^{pp'} I_J^{pp'} \mathcal{M}^{pp'}(IM; JM), \quad (23)$$

where

$$I_J^{pp'} = \int \Phi_J^{pp'}(\mathbf{r}_e, \mathbf{r}_h, \mathbf{r}, \mathbf{r}) \phi(\mathbf{r}_e, \mathbf{r}_h) d^3 r_e d^3 r_h d^3 r. \quad (24)$$

The values of  $\mathcal{M}^{pp'}(IM; JM)$  are tabulated in Table I. The corresponding results for other polarizations can be obtained by invoking symmetry. We find that, for  $x$  and  $y$  polarizations,

$$J_{M'} \langle XX | P_x^+ | \chi \rangle_{IM} = \begin{cases} J_1 \langle XX | P_z^+ | \chi \rangle_{I1} \mathcal{N}(IM; JM') & \text{if } J=I=1 \\ J_0 \langle XX | P_z^+ | \chi \rangle_{I0} \mathcal{N}(IM; JM') & \text{otherwise,} \end{cases} \quad (25)$$

and

$$J_{M'} \langle XX | P_y^+ | \chi \rangle_{IM} = J_{M'} \langle XX | P_x^+ | \chi \rangle_{IM} \exp[i(M-M')\pi/2]. \quad (26)$$

The values of  $\mathcal{N}(IM; JM')$  are tabulated in Table II.

### III. RESULTS AND DISCUSSION

#### A. Exciton and biexciton energy levels

The calculated excitonic energy levels are plotted in Fig. 1. To our knowledge, this is the first time that  $L > 0$  excitonic states in the weak confinement regime are being obtained. The  $L=1$  excitons are especially interesting as these may be excited in infrared spectroscopy as well as in two-photon spectroscopy. Both these phenomena have recently received some experimental attention.<sup>33,34</sup> Further discussion of this will be taken up separately. The results presented, though given scaled by the exciton Rydberg ( $E_R$ ), correspond to an electron-hole mass ratio  $m_e/m_h = 0.28$  appropriate for CuCl (Ref. 35) with  $m_e = 0.5$  and  $m_h = 1.8$ .

The  $L=0$  biexciton energy levels, with and without the exchange interaction included, are plotted in Fig. 2. In the absence of the exchange interaction, the states are labeled by the symmetry under exchange of the electrons and holes as described in the previous section. These states have more degeneracy than expected from the conservation of the total angular momentum ( $J$ ). For example, the  $2--$  states with  $J=0, 1$ , and  $2$  all have the same energy giving a ninefold degenerate state. The exchange interaction mixes states of

TABLE I.  $\mathcal{M}^{pp'}(IM; JM)$ , appearing in Eq. (23) for the transition dipole moment from the exciton state  $|\chi\rangle_{IM}$  to the biexciton state  $|XX\rangle_{JM}$  for the  $z$  polarization.

$(I, M)$	$J, pp' \rightarrow 0, ++$	$0, --$	$1, -e$	$1, +-$	$1, -+$	$2, --$
0,0	0	0	$-\sqrt{2}$	-1	1	0
1,1	0	0	0	1	1	$\sqrt{2}$
1,0	1	$-1/\sqrt{3}$	0	0	0	$2\sqrt{2}/3$
1,-1	0	0	0	-1	-1	$\sqrt{2}$

the same total angular momentum  $J$  as well as lifts the degeneracy of the  $2--$  states with  $J=0, 1$ , and  $2$ .

We note that in the bulk semiconductors there is a large discrepancy between the best variational estimates of the biexciton binding energy and the experimental results. For example, in CuCl, the variational calculation of Akimoto and Hanamura<sup>36</sup> and Brinkman, Rice and Bell<sup>37</sup> gives a very low value of 11 meV compared to the experimental value of 32 meV (Ref. 35). This large discrepancy was not noticed at the time these calculations were reported as the electron-hole mass ratio known at that time was substantially smaller than the presently accepted values which led to a fortuitous agreement with experiments.

We find that a small part of this discrepancy may be attributed to the neglect of the electron-hole exchange interaction. To see this, we note that the lowest biexciton state is of

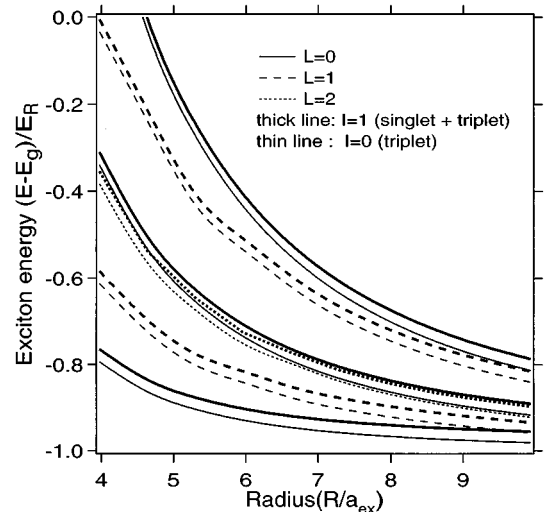


FIG. 1. Calculated energy levels of the  $L=0, 1$ , and  $2$  exciton states in semiconductor QD's.  $E_R$  is the exciton Rydberg,  $a_{ex}$  the exciton Bohr radius, and  $E_g$  is the bulk band gap energy.

TABLE II.  $\mathcal{N}(IM;JM')$ , appearing in Eq. (25) for the transition dipole moment from the exciton state  $|X\rangle_{IM}$  to the biexciton state  $|XX\rangle_{JM'}$  for the  $x$  polarization.

$(I,M)$	$J,M' \rightarrow$	0,0	1,0	1,1	1,-1	2,0	2, $\pm 1$	2,2	2,-2
0,0		0	0	$-1/\sqrt{2}$	$1/\sqrt{2}$	0	0	0	0
1,1		$-1/\sqrt{2}$	$1/\sqrt{2}$	0	0	$1/\sqrt{8}$	0	$-\sqrt{3}/2$	0
1,0		0	0	$1/\sqrt{2}$	$1/\sqrt{2}$	0	0	$-\sqrt{3}/8$	$\sqrt{3}/8$
1,-1		$1/\sqrt{2}$	$1/\sqrt{2}$	0	0	$-1/\sqrt{8}$	0	0	$\sqrt{3}/2$

$\Gamma_1$  symmetry because this state has its envelope function symmetric under exciton exchange and hence has a bonding character, like the bonding orbital of the hydrogen molecule, forming a bound state. As discussed in the last section, the electron-hole exchange interaction mixes the  $\Gamma_2 - \Gamma_2$  and the  $\Gamma_5 - \Gamma_5$  exciton product states that contribute to the  $\Gamma_1$  biexciton states and hence the biexciton ground state has an exchange contribution less than twice the exciton exchange energy. The experimentally quoted biexciton binding energy is the difference between twice the energy of the  $\Gamma_5$  exciton and the biexciton ground state energy, while the theoretical value is calculated as the difference between twice the energy of the  $\Gamma_2$  exciton and the biexciton ground state energy.<sup>36,37</sup> Thus, inclusion of the electron-hole exchange interaction increases the biexciton binding energy. In the following we employ the former definition of the biexciton binding energy.

For the largest size considered ( $10a_{\text{ex}}$ ), we find that the biexciton energy is increased by about  $1.3\Delta E_{\text{exch}}^0$  while in bulk CuCl, the exchange correction is quoted to be

$1.6\Delta E_{\text{exch}}^0$ , obtained as a first-order perturbative estimate using an explicit variational wave function, by Bassani *et al.*<sup>38</sup> We use  $\Delta E_{\text{exch}}^0 = 4.4$  meV for CuCl.<sup>39</sup>

Nonetheless, the variationally calculated bulk biexciton binding energy is still substantially smaller than the experimental result. On the other hand, our calculation gives a biexciton binding energy of 30.3 meV for a CuCl QD of  $R=70$  Å. Although this is slightly smaller than the bulk value of 32 meV, we can say that there is substantial improvement over the older calculations in the bulk material.

In Fig. 3 we plot the size dependence of the calculated biexciton binding energy. The biexciton binding energy in CuCl QD's was recently measured by Masumoto *et al.*<sup>40</sup> This experimental result is also shown in Fig. 3. As the radius of the QD increases from 28 Å to 70 Å, we find that the biexciton binding energy decreases from  $0.257E_R$  (50 meV) to  $0.156E_R$  (30.3 meV), while the experimental result in the same size range varies from  $0.33E_R$  (64 meV) to  $0.216E_R$  (42 meV), which is somewhat larger than the calculated re-

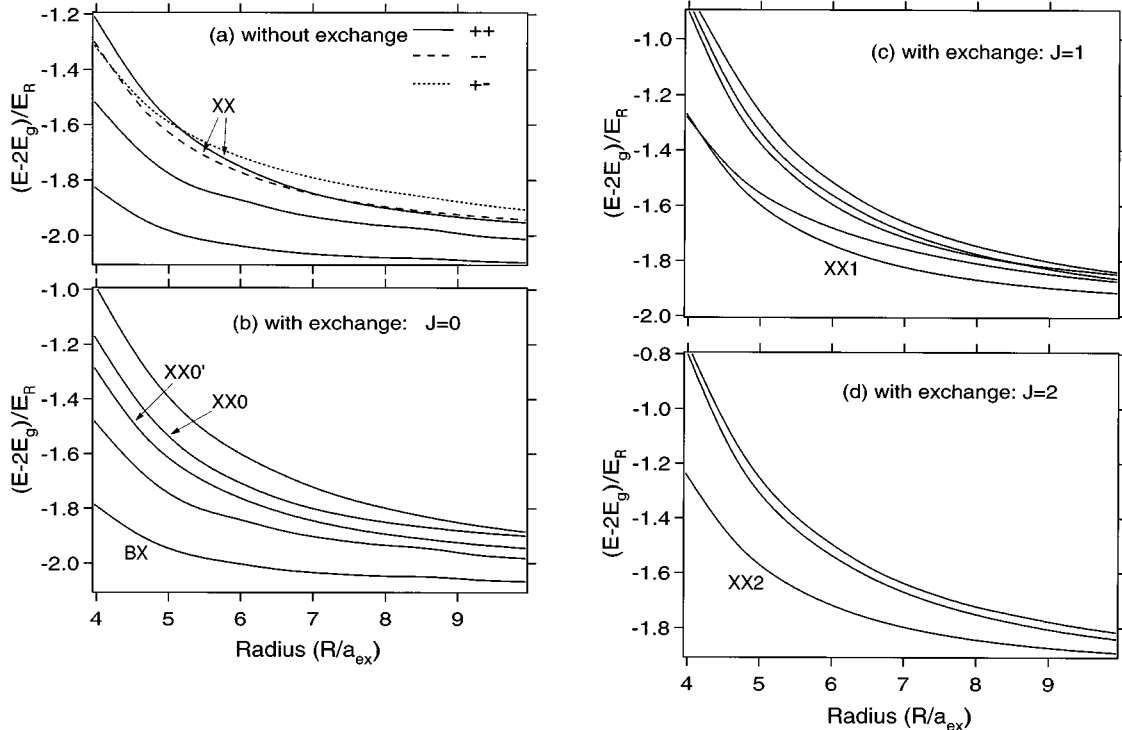


FIG. 2. Calculated energies of the biexciton states (a) without and (b–d) with the electron-hole exchange interaction included. BX, XX0 (XX0'), XX1, and XX2, respectively, denote the biexciton ground state and the weakly correlated exciton-pair states with  $J=0, 1$ , and  $2$ . Notations are the same as in Fig. 1.

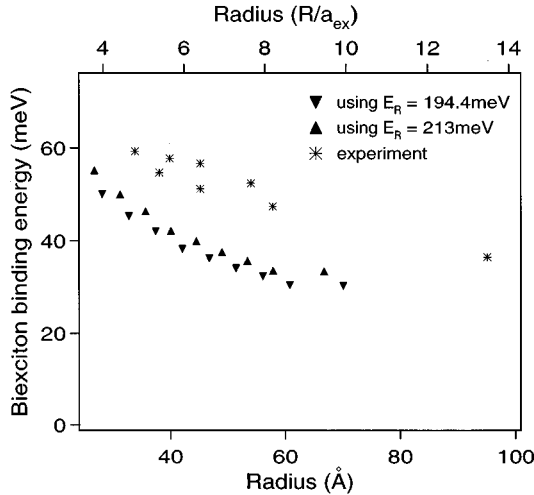


FIG. 3. The calculated size dependence of the biexciton binding energy in CuCl quantum dots. Two sets of results corresponding to the exciton Rydberg  $E_R=194.4$  meV and 213 meV are shown. The experimental results of Ref. 40 are also shown.

sult. These numbers correspond to  $E_R=194.4$  meV (Ref. 41) ( $a_{ex}=7.07$  Å). A proper comparison with the experiment is, however, made difficult by the lack of precise knowledge of the exciton Rydberg to be used and the size of the crystallites in the experimental sample. We show the calculated results corresponding to  $E_R=194.4$  meV as well as  $E_R=213$  meV, where the latter value is widely used in the literature on CuCl QD's (see, e.g., Ref. 40). As the experimentally estimated size<sup>40</sup> corresponds to matching the exciton energy to that predicted by the center of mass confinement picture, it is very sensitive to the values of the exciton mass, exciton Rydberg, and bulk exciton energy used. Keeping these reservations in mind, we find reasonable agreement between the experiment and the theory. The theory somewhat underestimates the biexciton binding energy possibly due to insufficient exciton-exciton correlation built into the wave function by the truncated basis set. However, the reasonable agreement with experiments indicates that the limited number of basis states used to make the problem numerically tractable do provide reliable results. The discrepancy between the theory and the experiment may also be partly attributed to the fact that the experimental sample contains somewhat flattened (platelet-shaped) crystallites<sup>42</sup> compared to the spherical shape that we consider.

Among the excited states of the biexciton, the most interesting ones are the nearly degenerate states occurring slightly above twice the ground state exciton energy. These states, marked XX in Fig. 2(a) and XX0, XX1, and XX2 in Figs. 2(b)–2(d), have an envelope function well approximated by the product of two ground state excitons. Consideration of the oscillator strengths for the exciton to biexciton transitions offers further important insights into the nature of these weakly correlated exciton-pair states. We therefore defer a detailed discussion of these excited biexciton states to be taken up later.

### B. Oscillator strengths

The physical nature of the biexcitonic states and their relevance to optical response become clearer on considering the

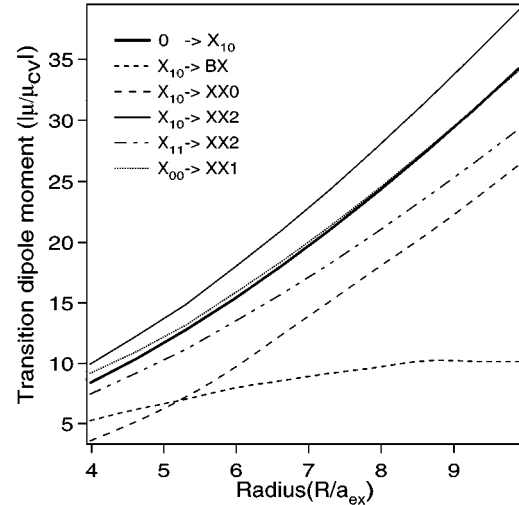


FIG. 4. Transition dipole moments for excitation of the lowest  $I=1$  exciton state ( $X_{10}$ ) and for the dominant transitions from the lowest exciton to the biexciton states. The biexciton states involved in the transitions are indicated by the energy level labels used in Fig. 2. 0 denotes the ground state and  $X_{I_z}$  denotes the lowest  $I=0$  or  $I=1$  exciton state.

oscillator strengths for their excitation from the excitonic states. In what follows we actually discuss only the transition dipole moments. The oscillator strength  $f$  of a transition is related to the transition dipole moment  $\mu$  through  $f=2m_0E|\mu|^2/e^2\hbar$ , where  $E$  is the energy of the transition.

Only the  $\Gamma_5$  ( $I=1$ ) excitons are optically excited from the ground state. As the  $\Gamma_5$  exciton state is threefold degenerate, subsequent excitation of the biexciton states will be dependent on the polarization of the exciton state. In Fig. 4, we plot the dipole moments for transitions from the  $\Gamma_5$  exciton ground state with  $I_z=0, \pm 1$ , to the biexciton states. Only a few dominant transitions are shown, and the dipole moment for excitation of the exciton ground state is also shown for comparison. The light polarization is taken to be along the  $z$  axis. In Fig. 5 we plot the squared dipole moments for the exciton to biexciton transitions as a function of the transition frequency for a few different values of the radius. While the limited data shown in Fig. 4 illustrate the size dependence of the dipole moments as discussed in detail below, Fig. 5 provides a complementary picture suitable for describing excited state absorption, discussed later.

As shown in the previous section, for the  $z$  polarization, only the  $I=1$ ,  $I_z=0$  exciton states can be excited by one-photon absorption from the ground state, while only the  $J=0$ ,  $J_z=0$ , and  $J=2$ ,  $J_z=0$  biexciton states are excited by a subsequent one-photon absorption. We note that this process is sufficient to discuss excitation of biexciton states by a two-step absorption of linearly polarized photons by the ground state. While experiments measuring the coherent nonlinear optical susceptibility, for example, are described by such processes, a pump-probe experiment could probe exciton and biexciton excitations by different polarizations. The latter case is discussed later.

The dipole moment for the transition from the biexciton ground state to the exciton, commonly referred to as the  $M$ -line emission, increases with the radius of the QD at small

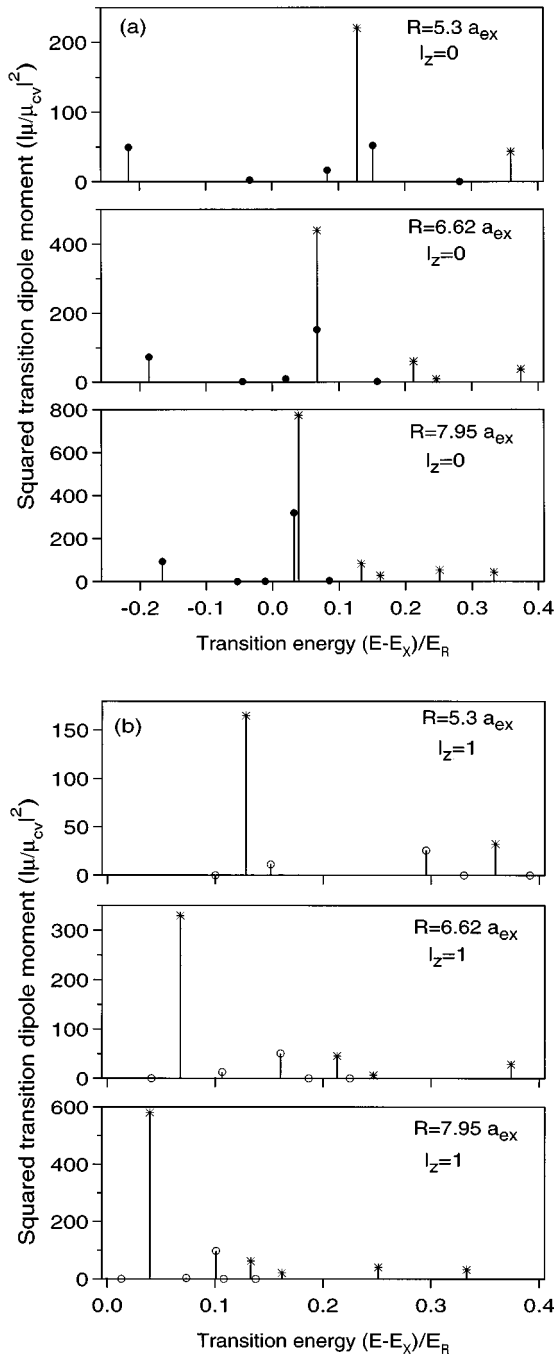


FIG. 5. Squared transition dipole moments for transitions from the lowest  $I=1$  exciton to the  $J=0, 1$ , and  $2$  biexciton states, respectively, marked by  $\bullet$ ,  $\circ$ , and  $*$ . Transitions from both (a)  $I_z=0$  and (b)  $I_z=1$  sublevels of the exciton are shown. The polarization of light is taken to be along the  $z$  axis.

sizes, but saturates towards the bulk value at larger sizes. For  $R=10a_{\text{ex}}$ , the  $M$ -line dipole moment of  $10.2\mu_{\text{cv}}$  corresponds to an oscillator strength of  $\approx 1900f_{\text{bulk}}$  for CuCl, which may be compared with the measured bulk value of  $2500f_{\text{bulk}}$ .<sup>43</sup> Here  $f_{\text{bulk}}$  is the oscillator strength per unit cell of the bulk  $\Gamma_5$  exciton.

While the exciton oscillator strength is proportional to the volume of the crystallite, provided the exciton envelope function is coherent over the whole crystallite, the biexciton

oscillator strength tends towards a constant value in the bulk limit. This behavior may be understood by the following simple physical argument. The creation of a biexciton from an exciton state involves the creation of a second exciton spatially close to the first one, within the volume of the biexciton. Thus in the bulk limit, the  $M$ -line oscillator strength is of the order of the exciton oscillator strength corresponding to a coherence volume equal to the volume of the biexciton. This is a constant, dictated by the size of the biexciton.

The calculated  $M$ -line oscillator strength corresponds to a radiative decay time of 660 psec for  $R=28 \text{ \AA}$ , gradually decreasing to 175 psec as the radius of the QD increases to  $70 \text{ \AA}$ . This may be compared with the measured biexciton decay time of 50 psec in bulk CuCl (Ref. 44) and 70 psec in CuCl nanocrystals of  $42 \text{ \AA}$  radius.<sup>45</sup> The above decay times for the QD are calculated assuming a host dielectric constant of 2.25, appropriate for glass. Even for the largest size considered by us, the radiative decay time is significantly larger than the bulk value because of the smaller dielectric constant of the host material compared to that of bulk CuCl and also because our calculated biexciton oscillator strength in the large  $R$  limit is somewhat smaller than the bulk value. The above discrepancy between the theory and experiments may also be attributed to the participation of nonradiative processes in actual samples. On the other hand, the mesoscopic enhancement of the exciton oscillator strength implies that the radiative decay time of the exciton is inversely proportional to the volume of the QD. For the exciton ground state, we find a decay time of 740 psec for  $R=28 \text{ \AA}$  decreasing to 45 psec for  $R=70 \text{ \AA}$  with good correspondence with experimental data.<sup>15</sup>

The most interesting result of the present calculation is the existence of the two nearly degenerate excited biexciton states (labeled  $XX0$  and  $XX2$  in Fig. 2) with a large oscillator strength as is evident from Fig. 4. These states have oscillator strengths increasing proportional to the QD volume, and the sum of their oscillator strengths approximately equals twice that of the exciton, especially at large sizes. For linearly polarized excitation, the states that share such a large oscillator strength have  $J=0$  and  $J=2$ ,  $J_z=0$ . Interestingly, we find that the wave functions of these states are well approximated by a product of two independent ground state exciton states, especially at larger sizes. Because of their large oscillator strength, these states will dominate the excited-state absorption as well as crucially influence the excitonic optical nonlinearity as discussed in the subsequent sections. Therefore a detailed consideration of these weakly correlated exciton-pair states is in order.

### C. Weakly correlated exciton-pair states

Let us consider the creation of a second exciton in a QD much larger in size than the exciton. Such a process will be most efficient when the second exciton is created uncorrelated with the first one, as it then would have an oscillator strength of the same order as that of creating a single exciton. Such an uncorrelated exciton pair can be an approximate eigenstate of a large QD because the exciton-exciton interaction is short ranged (dipole-dipole like), unlike the electron-hole interaction in an exciton. We may, in fact, construct two such excited states with almost the same energy,

$$\begin{aligned} \Phi_{XX}^{\pm\pm} = & (1/\sqrt{2})[\phi_X^g(\mathbf{r}_{e1}, \mathbf{r}_{h1})\phi_X^g(\mathbf{r}_{e2}, \mathbf{r}_{h2}) \\ & \pm \phi_X^g(\mathbf{r}_{e1}, \mathbf{r}_{h2})\phi_X^g(\mathbf{r}_{e2}, \mathbf{r}_{h1})], \end{aligned} \quad (27)$$

where  $\phi_X^g$  is the envelope function of the exciton ground state.

In the limit of large  $R$  these two states ( $++$  and  $--$ ) have a combined oscillator strength and energy twice those of the exciton ground state. The exchange interaction splits these into four states, two with  $J=0$ , and one each with  $J=1$  and  $J=2$ . The corresponding wave functions are given by

$$\Psi_{XX0} = \frac{\sqrt{3}}{2}\Phi_{XX}^{++}\chi_{00}^{00} - \frac{1}{2}\Phi_{XX}^{--}\chi_{00}^{11}, \quad (28a)$$

$$\Psi_{XX0'} = \frac{1}{2}\Phi_{XX}^{++}\chi_{00}^{00} - \frac{\sqrt{3}}{2}\Phi_{XX}^{--}\chi_{00}^{11}, \quad (28b)$$

$$\Psi_{XX1} = \Phi_{XX}^{--}\chi_{1M}^{11}, \quad (29)$$

$$\Psi_{XX2} = \Phi_{XX}^{--}\chi_{2M}^{11}, \quad (30)$$

where Eq. (28) is obtained by diagonalizing Eq. (13) in the subspace of the two functions given by Eq. (27). The diagonalization is achieved by noting that integrals involving cross terms like  $\phi_X^g(\mathbf{r}, \mathbf{r})\phi_X^g(\mathbf{r}_{e2}, \mathbf{r}_{h2})\phi_X^g(\mathbf{r}, \mathbf{r}_{h2})\phi_X^g(\mathbf{r}_{e2}, \mathbf{r})$  tend to zero as  $R \rightarrow \infty$ . Only two of these,  $XX0$  and  $XX2$  (respectively, with  $J=0$  and  $J=2$ ) are excited by multistep excitation via the  $I=1$  exciton ground state. Both these states have an exchange energy of twice that of the exciton ground state. The dipole moments for excitation of these states may be calculated using Eqs. (23), (24), and Table I. Noting that the second term in Eq. (27) makes a negligible contribution to the integral in Eq. (24), it follows that the transition dipole moments for excitation of the states  $XX0$  and  $XX2$ , respectively, equal  $\sqrt{2/3}$  and  $\sqrt{4/3}$  times that of the exciton ground state. Thus, in the limit of large  $R$  the states  $XX0$  and  $XX2$  will have a combined oscillator strength of twice that of the exciton ground state. For finite  $R$ , the exciton-exciton interaction would modify this picture, but our numerical results agree with the above description, to a good approximation, especially at larger sizes. The four weakly correlated exciton-pair states  $XX0$ ,  $XX0'$ ,  $XX1$ , and  $XX2$ , described above are shown in Figs. 2(b)–2(d).

It is interesting to note that the factor of two in the oscillator strength may also be understood as the bosonic enhancement factor corresponding to the creation of a second identical exciton. It would be interesting to extend this picture to the creation of multiple-exciton states in large QD's. We note that the independent boson picture implicit in this argument is reasonable as long as the QD is large enough to accommodate the excitons without a considerable overlap. Further investigation of this aspect is left for future study. Experimentally, QD's provide a unique opportunity of creating a definite number of excitons in a small and well-defined volume allowing the observation of the bosonic enhancement in the exciton creation.

As the size of the QD is reduced, the two excitons overlap with each other, the state corresponding to  $\Phi_{XX}^{--}$  acquiring a repulsive energy as is well known with the case of the anti-bonding state of the hydrogen molecule. On the other hand, the  $\Phi_{XX}^{++}$  state gets more and more mixed with and repelled by the biexciton ground state. The net effect of this size dependent evolution of the weakly correlated exciton-pair states is a weakening of their oscillator strength as well as a blueshift of the corresponding exciton-biexciton transition, as the QD size is reduced.

In addition to those discussed above, we also find a  $J=1$  weakly correlated product state [labeled  $XX1$  in Fig. 2(c)], which corresponds to the product of the  $I=0$  ( $\Gamma_2$ ) and  $I=1$  ( $\Gamma_5$ ) exciton ground states. As  $\Gamma_2$  excitons are not optically excited, this state cannot be excited by absorption of two identically polarized photons. However, it can be excited by the absorption of, for example, a  $z$ -polarized photon from the  $I=1$ ,  $I_z = \pm 1$ , or the  $I=0$  states. The latter process has a dipole moment comparable to that of the exciton, and is also shown in Fig. 4.

## IV. NONLINEAR OPTICAL PROPERTIES

### A. Size dependence of the third-order nonlinear susceptibility

As discussed above, the weakly correlated exciton-pair states have a large oscillator strength. As the excitonic and two-excitonic contributions to the third-order nonlinear susceptibility have opposite signs, the weakly correlated state would play a crucial role in determining the resonant excitonic nonlinearity in large QD's. We shall now investigate this in detail.

The third-order nonlinear susceptibility,  $\chi^{(3)}(-\omega; \omega, \omega, -\omega)$  may be obtained from perturbation theory as<sup>46</sup>

$$\begin{aligned} \chi^{(3)}(-\omega; \omega, \omega, -\omega) = & -iN \sum_{e,b} \frac{|\mu_{eg}|^2}{2\hbar^3 \gamma_{eg}^e} \frac{\gamma_{eg}}{(\omega_{eg} - \omega)^2 + \gamma_{eg}^2} \left[ \frac{2|\mu_{eg}|^2}{i(\omega_{eg} - \omega) + \gamma_{eg}} - \frac{|\mu_{be}|^2}{i(\omega_{be} - \omega) + \gamma_{be}} \right] \\ & - iN \sum_{e,b} \frac{i|\mu_{eg}|^2 |\mu_{be}|^2}{4\hbar^3} \frac{1}{i(\omega_{eg} - \omega) + \gamma_{eg}} \frac{1}{i(\omega_{bg} - 2\omega) + \gamma_{bg}} \left[ \frac{1}{i(\omega_{eg} - \omega) + \gamma_{eg}} - \frac{1}{i(\omega_{be} - \omega) + \gamma_{be}} \right], \end{aligned} \quad (31)$$

where we have retained only the near-resonant terms. Here,  $\hbar\omega_{ij}$ ,  $\mu_{ij}$ , and  $\gamma_{ij}$ , respectively, denote the energy, dipole moment, and dephasing rate corresponding to a transition between the states  $i$  and  $j$ . The subscripts  $g$ ,  $e$ , and  $b$ , denote the ground state, the exciton states, and the biexciton states, respectively.  $\gamma_{\parallel}^e$  denotes the exciton population decay rate and  $N$  is the number density of the quantum dots.

The first two terms in Eq. (31) arise from the saturation of the exciton population while that last two terms arise from the two-photon coherence of the biexciton state. Thus there will be resonant enhancement of  $\chi^{(3)}$  at the exciton to biexciton transition energy as well as at the exciton energy. The former case is especially interesting as the increase in  $\chi^{(3)}$  is not accompanied by an increase in absorption, unlike at the exciton resonance. Consequently, the dynamics at this two-photon resonance would be governed by the dephasing time of the biexciton and thus promise a fast response time. However, as the QD size increases, the oscillator strength of the bound biexciton saturates towards a constant value and shows no mesoscopic enhancement. On the other hand, in the weak confinement regime that we consider, the mesoscopically enhanced exciton oscillator strength would lead to mesoscopic enhancement of  $\chi^{(3)}$ .

In fact, the resonant excitonic  $\chi^{(3)}$  of CuCl QD's has been observed<sup>10</sup> to increase with the radius of the QD, exhibiting such a mesoscopic enhancement. But as  $R$  is increased to about 50 Å (at 77 K),  $\chi^{(3)}$  was seen to saturate and then to rather abruptly decrease with a further increase in  $R$ . This size dependence has never been explained satisfactorily. We shall see below that this saturation of the excitonic contribution to  $\chi^{(3)}$  and the reversal of its size dependence arise from competing contributions from the weakly correlated exciton-pair states and from the exciton ground state. The weakly correlated exciton-pair states also have mesoscopically enhanced oscillator strengths and a proper consideration of the size dependence of  $\chi^{(3)}$  should include a contribution from such states, as described by Eq. (31).

Now we consider the size dependence of the mesoscopically enhanced  $\chi^{(3)}$  at the lowest exciton resonance. As there will be considerable linear absorption at the exciton resonance it would be appropriate to consider the figure of merit  $\eta = |\chi^{(3)}|/\alpha$ , where  $\alpha$  is the linear absorption coefficient given by

$$\alpha(\omega) = N \frac{\omega}{nc} \frac{4\pi}{\hbar} \sum_e \frac{|\mu_{eg}|^2 \gamma_{eg}}{(\omega - \omega_{eg})^2 + \gamma_{eg}^2}, \quad (32)$$

where  $n$  is the refractive index of the sample which, for a dilute collection of QD's, may be approximated by that of the host material. Following the experimental results of Refs. 10 and 14 on CuCl QD's, the size dependence of  $\gamma_{\parallel}^e$  and  $\gamma_{eg}$  are fitted as

$$\gamma_{eg} = \begin{cases} 0.04(45 - R) + \gamma_h & \text{if } R \leq 45 \text{ \AA} \\ \gamma_h & \text{if } R > 45 \text{ \AA}, \end{cases} \quad (33a)$$

$$\frac{1}{\gamma_{\parallel}^e} = \tau = 1.07 \times 10^6 R^{-2.26}, \quad (33b)$$

where  $R$  is in angstroms,  $\gamma_{eg}$  is in meV, and  $1/\gamma_{\parallel}^e$  is in psec, and this form is assumed for all the exciton levels. Although

$\gamma_h$  that appears in Eq. (33a) is reported to be 0.9 meV,<sup>10</sup> we treat it as a free parameter and discuss the dependence of  $\chi^{(3)}$  on  $\gamma_h$ . In the absence of experimental information on the homogeneous linewidth of the biexciton states, we take it to be the same as that of the exciton.

In Fig. 6(a) we plot the maximum value of the  $|\chi^{(3)}|/\alpha$  as a function of the radius of the QD. In the calculation of  $\chi^{(3)}$ , we include the lowest four  $L=0$  exciton levels and five lowest energy biexciton states each with  $J=0, 1$ , and  $2$ . Here we use material parameters appropriate for CuCl (Ref. 41) and take  $n=2.25$ , appropriate for glass matrix. In the size range considered, the peak value of  $\chi^{(3)}$  occurs almost exactly at the exciton resonance frequency. Several values of  $\gamma_h$  are considered. For a small value of  $\gamma_h$  (less than a meV),  $\eta$  increases at small sizes sublinearly with  $R$ , the rate of increase slightly decreasing as  $R$  increases to  $10a_{ex}$ . This is easily understood as the size dependence of the dominating resonant excitonic contribution to  $\chi^{(3)}$ , determined by the exciton oscillator strength increasing as  $R^3$  and the population decay time  $\tau$  decreasing as  $R^{-2.26}$ . But, as  $\gamma_h$  is increased, this behavior dramatically changes. We find that at the radius for which  $\gamma_h$  becomes comparable to the energy difference  $\delta E = E_{XX0} - 2E_X$  or  $E_{XX2} - 2E_X$ , the size dependence of  $\chi^{(3)}$  tends to saturate and, interestingly,  $\chi^{(3)}$  decreases with a further increase in  $R$ . This correspondence between  $\gamma_h$  and the size dependence of the energy difference ( $\delta E$ ) is illustrated in Fig. 6(b). For the case of  $\gamma_h = 3$  meV, the size at which  $\delta E \approx \gamma_h$  is estimated to be  $R = 68$  Å and this value is in good agreement with the radius at which  $\chi^{(3)}/\alpha$  shows a maximum in Fig. 6(a).

This behavior may be easily understood as arising from the weakly correlated exciton-pair state which makes a competing contribution to  $\chi^{(3)}$  and tends to cancel the strong

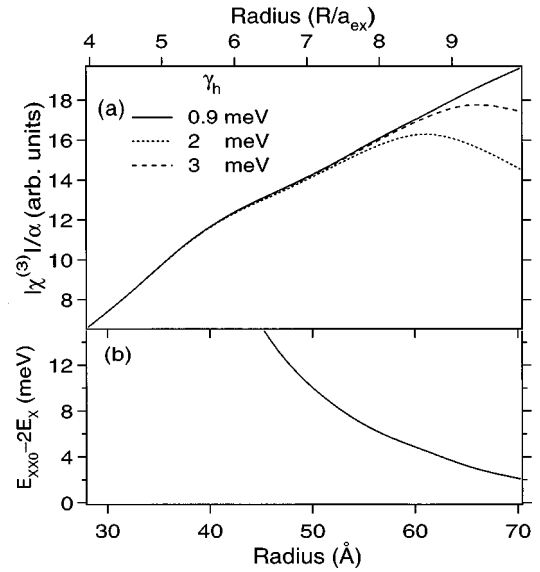


FIG. 6. (a) Calculated size dependence of the peak value of  $|\chi^{(3)}|/\alpha$  near the exciton resonance in CuCl QD's. All the curves are scaled to the same value at  $R=28$  Å. The hump seen at  $R \approx 40$  Å arises from the assumed size dependence of  $\gamma_h$  and has no special physical significance. (b) The size dependence of the energy difference between the weakly correlated exciton-pair state ( $E_{XX0}$ ) and twice the exciton ground state energy ( $E_X$ ).

excitonic contribution. In very small QD's where the electron-hole correlation is negligible,  $\chi^{(3)}$  arises from the atomiclike level filling mechanism, while in the bulk semiconductor one would have excitons behaving like independent bosons strongly suppressing the excitonic contribution to  $\chi^{(3)}$ . The presence of the weakly correlated exciton-pair states with nearly twice the exciton energy and with nearly twice the exciton oscillator strength that we have identified in large QD's implies an approach to such a bulklike behavior.

An explicit demonstration of this cancellation between excitonic and two-excitonic contributions may be presented using a three-level model. In the present case of a three-level model consisting of the ground state, the lowest exciton state, and the weakly correlated two-exciton state, there are two competing contributions to  $\chi^{(3)}/\alpha$  proportional to<sup>47</sup>

$$\frac{2|\mu_X|^2}{(\omega_X - \omega) - i\Gamma} - \frac{|\mu_{XX}|^2}{(\omega_{XX} - \omega) - i\Gamma}, \quad (34)$$

where the three levels are labeled by 0, X, and XX, and  $\omega_X$  and  $\omega_{XX}$  denote the transition frequencies and  $\mu_X$  and  $\mu_{XX}$  the dipole moments for the transitions  $0 \rightarrow X$  and  $X \rightarrow XX$ , respectively.  $\Gamma$  denotes the homogeneous widths of these transitions. The two terms in Eq. (34) exactly cancel when  $|\mu_{XX}|^2 = 2|\mu_X|^2$  and  $\omega_X = \omega_{XX}$ , a situation to which the QD level structure is found to approach as  $R$  increases.

In actual samples, there is also inhomogeneous broadening, probably due to size and shape inhomogeneities of the microcrystals. In Fig. 7, we show the size dependence of  $|\chi^{(3)}|/\alpha$  for different values of homogeneous and inhomogeneous broadening of the exciton and biexciton states. In the absence of detailed information on the inhomogeneous broadening we assume a phenomenological Gaussian inhomogeneous broadening with a common width  $\gamma_{ih}$  for all the one-photon transition frequencies,  $\omega_{eg}$  and  $\omega_{be}$ . Then the average over the inhomogeneous broadening is equivalent to that over the excitation photon energy and we have the average  $\chi^{(3)}$  given by

$$\int \chi^{(3)}(-\omega'; \omega', \omega', -\omega') \exp[-(\omega - \omega')^2 / \gamma_{ih}^2] d\omega'. \quad (35)$$

A similar averaging is done for  $\alpha$ . Increasing the inhomogeneous width causes the saturation radius to shift to lower values. We note that, the experimentally measured value of  $\gamma_h = 0.9$  meV<sup>10</sup> for  $R > 50$  Å is somewhat too small to cause the strong saturation observed around  $R = 50$  Å<sup>10</sup> unless considerable inhomogeneous broadening is also present.

While the data shown in Figs. 6 and 7 are given in arbitrary units, it is interesting to compare the absolute value of  $\chi^{(3)}$  with experiments. Using the bulk exciton oscillator strength for CuCl to be  $5.85 \times 10^{-3}$  per unit cell,<sup>44</sup> we find that  $|\chi^{(3)}|/\alpha = 2.7 \times 10^{-9}$  esu cm, in a crystallite of 37.4 Å radius. We have used  $\gamma_h = 0.9$  meV. This is in close agreement with the measured value of  $3.4 \times 10^{-9}$  esu cm.<sup>10</sup>

### B. II-VI semiconductor QD's

Although most experiments in the weak confinement regime are done on CuCl quantum dots, optical properties of

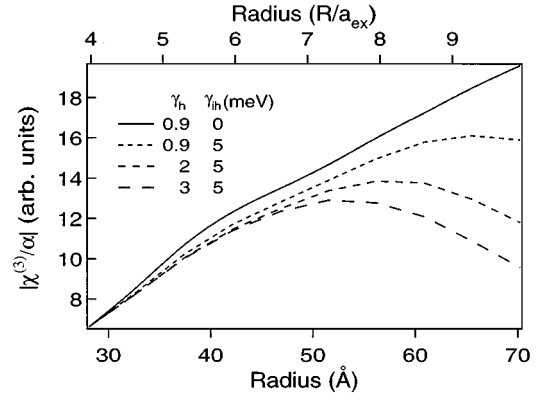


FIG. 7. Same as Fig. 6(a), but with inhomogeneous broadening ( $\gamma_{ih}$ ) included.

QD's of II-VI semiconductors like CdS and CdSe have been widely studied since the early days of quantum dot research. It is, therefore, interesting to apply our results to materials like CdS and CdSe. Although the present calculation uses an electron-hole mass ratio of 0.28, appropriate for CuCl, the results would be expected to be applicable to many other materials because of the weak dependence of exciton and biexciton states on the electron-hole mass ratio.<sup>3</sup> In fact, the electron-hole mass ratios of 0.23 for CdS (Ref. 41) and 0.28 for CdSe (Ref. 41) are very close to that of CuCl.

For CdS, taking  $a_{ex} = 30$  Å and  $E_R = 29$  meV,<sup>41</sup> we note that a homogeneous width  $\gamma_h = 2$  meV ( $= 0.067E_R$ ) would lead to the saturation of  $\chi^{(3)}$  to occur at a size corresponding to  $\delta E \approx 0.067E_R$ . Referring to Fig. 6(b) and scaling the energies by  $E_R = 194.4$  meV, we find that this corresponds to  $R \approx 6.5a_{ex}$  or about 200 Å. For CdSe, taking  $E_R = 15.7$  meV,<sup>41</sup> we get the same value of saturation radius,  $6.5a_{ex}$ , with a homogeneous broadening of only 1 meV. Thus, in materials with smaller exciton binding energy, the effect of the weakly correlated exciton-pair states becomes important at smaller values of  $R/a_{ex}$ , unless the exciton linewidth is also correspondingly smaller.

Different experimental measurements of the size dependence of  $\chi^{(3)}$  in CdSe and CdS<sub>x</sub>Se<sub>1-x</sub> QD's have reported conflicting results.<sup>48</sup> A recent careful analysis of these results by Schanne-Klein *et al.*<sup>49</sup> has related this behavior to the difference between fresh and photodarkened samples and has shown that the excitonic contribution to  $\chi^{(3)}$  is an increasing function of  $R$ . They observed that the figure of merit  $\chi^{(3)}/\alpha\tau$  in CdSe QD's is enhanced by a factor of 4.4 as the radius increases from 27 Å to 44 Å. The experimentally studied size range is much smaller than the size at which we expect the weakly correlated exciton-pair states to suppress the mesoscopic enhancement of  $\chi^{(3)}$ . Therefore, we may expect a further enhancement of the figure of merit in larger QD's. It is, however, difficult to make a quantitative prediction of the optimal size at which the figure of merit is maximized, because of insufficient knowledge on the homogeneous linewidths of the exciton and biexciton in these materials. In light of the present result, experimental investigation of CdS and CdSe crystallites of larger sizes would be interesting. It is important to note the physics of the weakly correlated exciton-pair states elucidated above is

quite general and details of the valence band symmetries and exchange interaction play only a minor role.

### C. Excited-state absorption from the exciton ground state

There is a growing interest in size selective spectroscopy of semiconductor crystallites. Recent progress in experiments has revealed the discrete energy level structures not only in the excitation spectrum<sup>50,51</sup> but also in the excited state absorption spectra by a resonant pump-probe technique.<sup>52</sup> Using the exciton and biexcitonic states calculated above, we can now theoretically predict the absorption spectra of excited crystallites in which one exciton has already been created.

We consider a pump-probe experiment in which a linearly polarized pump pulse excites a crystallite into the exciton ground state and a collinear probe pulse that follows probes the absorption spectra of this excited crystallite. We take the pump-probe propagation direction to be the  $x$  axis and the pump polarization to be along the  $z$  axis, without a loss of generality. The created exciton is in the  $I=1$  ( $\Gamma_5$ ) state with  $I_z=0$ . Subsequent absorption of a probe photon can then excite the  $J=0$ , and  $J=2$ ,  $J_z=0$  two-exciton states if the probe is  $z$  polarized, and the  $J=1$ ,  $J_z=\pm 1$ ,  $J=2$ , and  $J_z=\pm 1$  two-exciton states if the probe is  $y$  polarized. The oscillator strengths for all these processes can be calculated using the expressions given in Sec. II D.

In Fig. 8, we plot the oscillator strengths for transitions from the exciton ground state assuming the probe to be unpolarized. As expected from the large oscillator strength of the weakly correlated exciton-pair states, we find them to dominate the excited state absorption. The lowest energy absorption peak redshifted from the exciton energy corresponds to the biexciton ground state. There are a few weak transi-

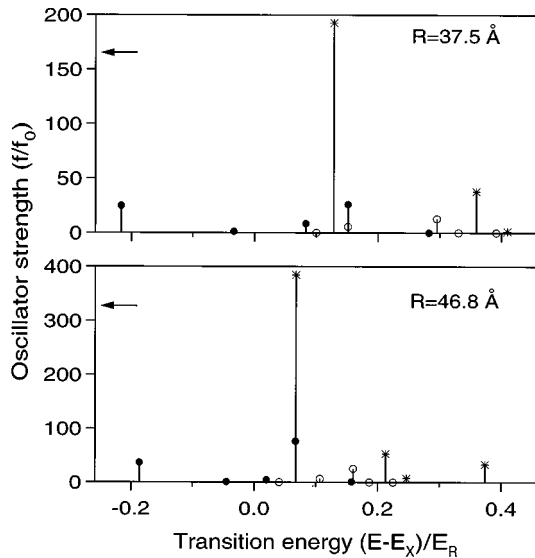


FIG. 8. Oscillator strengths ( $f$ ) for the induced absorption from the  $I=1$ ,  $I_z=0$  exciton ground state by an unpolarized probe beam. ●, ○, and \*, respectively, denote transitions to the  $J=0$ ,  $J=1$ , and  $J=2$  biexciton states.  $f_0=2m_0|\mu_{cv}|^2E/e^2\hbar$ , where  $E$  is the energy of the transition and  $E_X$  is the exciton ground state energy. The arrows indicate the oscillator strength of the exciton ground state.

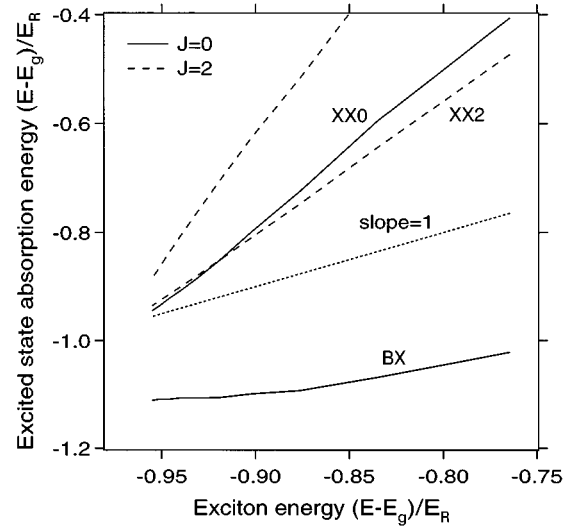


FIG. 9. Energies of the dominant excited-state absorption peaks appearing in Fig. 8 as a function of the exciton ground state energy. BX, XX0, and XX2 denote transitions to the biexciton ground state and to the weakly correlated exciton-pair states with  $J=0$  and 2, respectively. The dotted line is a line of slope 1 and is only shown for reference.

tions to the excited, but bound, biexciton states occurring below the exciton energy. The strong absorption peaks due to excitation of the  $J=0$  and  $J=2$  weakly correlated pair states (XX0 and XX2) occur blueshifted from the exciton. We argue that the experimentally observed blueshift of the probe absorption in the presence of a strong pump beam<sup>17</sup> involves excitation of such exciton-pair states. For  $R=47$  Å, the blueshift is found to be 11.5 meV and these transitions have a combined oscillator strength of about 1.3 times that of the exciton ground state. This result agrees very well with the measured blueshift of about 10 meV for  $R\approx 45$  Å.

In Fig. 9 we plot the energies of a few dominant excited-state absorption peaks as a function of the exciton ground state energy, i.e., the pump photon energy. It is interesting to note that the strongest excited-state absorption to the  $J=2$  two-exciton state shown in Fig. 9, has a linear dependence on the exciton ground state energy with a slope of about 2.4. Although the origin for this rather simple relationship is not clear, it is amusing to speculate, by invoking the center of mass confinement picture, that the weakly correlated exciton pair has an energy equal to that of two excitons independently confined in a region of half the volume of the QD. Such a picture gives the confinement kinetic energy of the weakly correlated pair to be  $2\sqrt[3]{4}=3.174$  times that of a single exciton. Consequently, the corresponding excited-state absorption energy will be linearly dependent on the exciton energy with a slope of about 2.2, in close agreement with the actual value.

Recently, Masumoto and co-workers<sup>52</sup> observed fine structures in the excited-state absorption spectrum and the features in the observed spectrum agree well with that expected from the present calculation. In their pump-probe experiments with the pump tuned to the exciton absorption energy, they observed a strong excited-state absorption of the probe, blueshifted from the pump energy, in addition to the biexciton absorption. The strength of the induced absorption

to this excited two-exciton state is found to be several times larger than that to the biexciton ground state as expected from the above discussion.

## V. SUMMARY AND CONCLUSIONS

We have presented a calculation of the excitonic and biexcitonic states in semiconductor QD's of radii up to 10 times the exciton Bohr radius. The most important finding of the present calculation is the presence of excited biexciton states with large oscillator strengths, which play a crucial role in determining the nonlinear optical properties of QD's in the weak confinement regime. These states are identified to consist of two weakly correlated ground state excitons and consequently have oscillator strengths, for excitation from the exciton ground state, increasing proportional to the volume of the QD. In fact, the combined oscillator strength of the nearly degenerate  $J=0$  and  $J=2$  weakly correlated two-exciton states is found to be nearly twice that of the exciton ground state. These states also have their energies close to twice that of the exciton ground state. Consequently, the two-pair states give rise to a competing contribution to the mesoscopically enhanced  $\chi^{(3)}$  at the exciton resonance, leading to a saturation and reversal of the size dependence of  $\chi^{(3)}$ . This provides the first consistent understanding of the experimentally observed<sup>10</sup> size dependence of  $\chi^{(3)}$  in CuCl QD's. This mechanism of the saturation of the mesoscopically enhanced  $\chi^{(3)}$  is of quite fundamental character and is applicable to other materials.

The excited-state absorption from the exciton ground state has also been investigated. Again, the excitation of the weakly correlated exciton-pair state is found to dominate the spectrum. As the size of the QD is reduced, these two-exciton states acquire a repulsive energy and we argue that the experimentally observed blueshift of the exciton absorp-

tion peak in the pump-probe experiment of Ref. 17 corresponds to excitation of the weakly correlated exciton-pair states. Our results are in good agreement also with the recent measurement of excited-state absorption spectra,<sup>52</sup> giving convincing evidence for the presence of the weakly correlated two-pair states.

The cancellation effect in  $\chi^{(3)}$  that sets in as the size of the QD increases indicates the approach towards a bosonic (harmonic) behavior of excitons in the low density regime. In the bulk limit, one would expect an exact cancellation of the resonant one-exciton and two-exciton contributions so that  $\chi^{(3)}$  is determined by nonresonant contributions from the bound biexciton and other excited two-exciton states. However, the cancellation referred to above may not be complete even in a harmonic approximation, because of possible differences in the dephasing rates of the one- and two-exciton states. Consequently, a calculation of the bulk limit of  $\chi^{(3)}$  at the exciton resonance requires careful consideration of the size dependence of the relaxation rates as well as of the off resonant contribution. This is left for future study. We note that similar conclusions have been reached by Belleguie and Bányai<sup>53</sup> by using an asymptotic model for the exciton-exciton interaction.

Finally, we note that the weakly correlated exciton-pair states identified here are of a quite general nature and would exist in other semiconductor structures like quantum wells and wires also. It would be interesting to investigate their effects on the optical response.

## APPENDIX A: TWO-PARTICLE STATES WITH $L=1,2$

Here we derive Eqs. (5) and (6). We may write a general two-particle wave function of angular momentum  $L$  and its  $z$  component  $M$  as

$$\phi_{LM}(\mathbf{r}_1, \mathbf{r}_2) = F(r_1, r_2, r_{12}) Y_{LM}(\Omega_1) + G(r_1, r_2, r_{12}) Y_{LM}(\Omega_2) + \sum_{ll'} g_{ll'}(r_1, r_2) \sum_m C_{m, M-m, M}^{l, l', L} Y_{lm}(\Omega_1) Y_{l', M-m}(\Omega_2), \quad (\text{A1})$$

where  $r_{12} = |\mathbf{r}_1 - \mathbf{r}_2|$ . Expanding  $F$  and  $G$  as

$$F(r_1, r_2, r_{12}) = \sum_l F_l(r_1, r_2) \sum_m (-1)^m Y_{lm}(\Omega_1) Y_{l, -m}(\Omega_2) \quad (\text{A2})$$

and similarly for  $G$ , and using

$$(-1)^m Y_{lm}(\Omega_1) Y_{L, M}(\Omega_2) = \sum_{l'm'} C_{m, -m', -M}^{ll'L} \sqrt{\frac{(2l+1)(2l'+1)}{4\pi(2L+1)}} Y_{l'm'}(\Omega_2), \quad (\text{A3})$$

we rewrite Eq. (A1) as

$$\phi_{LM}(\mathbf{r}_1, \mathbf{r}_2) = \sum_{ll'} \{ [F_{l'}(r_1, r_2) + G_l(r_1, r_2)] A_{ll'L} + g_{ll'}(r_1, r_2) \} \sum_m C_{m, M-m, M}^{l, l', L} Y_{lm}(\Omega_1) Y_{l', M-m}(\Omega_2), \quad (\text{A4})$$

where  $A_{ll'L} = C_{000}^{l,l',L} \sqrt{(2l+1)(2l'+1)/4\pi(2L+1)}$  is non-zero for all  $l, l'$  such that  $|l-l'| \leq L \leq (l+l')$  with  $l+l'+L$  even. Noting that only such  $l, l'$  values appear in the general form given by Eq. (4) for states with parity  $(-1)^L$ , in what follows we consider only such states.

Comparing Eq. (A4) with Eq. (4), we have

$$[F_{l'}(r_1, r_2) + G_l(r_1, r_2)]A_{ll'L} + g_{ll'}(r_1, r_2) = f_{ll'}(r_1, r_2). \quad (\text{A5})$$

For  $L=1$ , Eq. (A5) may be satisfied with  $g_{ll'}=0$ , by choosing

$$G_{l+2} = G_l + \frac{f_{l+2,l+1}}{A_{l+2,l+1,1}} - \frac{f_{l,l+1}}{A_{l,l+1,1}}, \quad (\text{A6a})$$

$$F_{l-1} = \frac{f_{l,l-1}}{A_{l,l-1,1}} - G_l. \quad (\text{A6b})$$

Then Eq. (A1) reduces to Eq. (5).

For  $L=2$ , Eq. (A5) gives

$$(G_l + F_{l+2})A_{l,l+2,2} + g_{l,l+2} = f_{l,l+2}, \quad (\text{A7a})$$

$$(G_l + F_{l-2})A_{l,l-2,2} + g_{l,l-2} = f_{l,l-2}, \quad (\text{A7b})$$

$$(G_l + F_l)A_{ll2} + g_{ll} = f_{ll}. \quad (\text{A7c})$$

Equation (A7a) and Eq. (A7b) can be satisfied with  $g_{l,l+2} = g_{l,l-2} = 0$  by choosing

$$G_{l+4} = G_l + \frac{f_{l+4,l+2}}{A_{l+4,l+2,2}} - \frac{f_{l,l+2}}{A_{l,l+2,2}} \quad (\text{A8a})$$

and

$$F_{l-2} = \frac{f_{l,l-2}}{A_{l,l-2,2}} - G_l, \quad (\text{A8b})$$

which leaves  $G_0, G_1, G_2, G_3$  arbitrary. Using Eq. (A8), Eq. (A7c) may be written as

$$\left( G_l + \frac{f_{l+2,l}}{A_{l+2,l,2}} - G_{l+2} \right) A_{ll2} + g_{ll} = f_{ll}. \quad (\text{A9})$$

Now we may choose  $G_0, G_1, G_2, G_3$  such that  $g_{ll}=0$  for  $l=0,1,2,3$ , but  $g_{ll}$  for  $l \geq 4$  cannot be made to vanish, in general. Thus we get Eq. (6) for the  $L=2$  state with even parity.

## APPENDIX B: ELECTRON-HOLE EXCHANGE INTERACTION

We derive the exciton and biexciton EMA equations including the electron-hole exchange interaction. We follow the treatment of Ref. 54 and start from an effective two-band Hamiltonian describing electrons and holes in a semiconductor:<sup>55</sup>

$$\begin{aligned} H = & \sum_{\mathbf{k}\sigma} E_c(\mathbf{k}) a_{\mathbf{k}\sigma}^\dagger a_{\mathbf{k}\sigma} - \sum_{\mathbf{k}\sigma} E_v(\mathbf{k}) b_{\mathbf{k}\sigma}^\dagger b_{\mathbf{k}\sigma} + \frac{1}{2} \sum_{\mathbf{k}_1 \mathbf{k}_2 \mathbf{k}_3 \mathbf{k}_4} \sum_{\sigma_1 \sigma_2} V_{\sigma_1 \sigma_2 \sigma_2 \sigma_1}^{cccc}(\mathbf{k}_1 \mathbf{k}_2 \mathbf{k}_3 \mathbf{k}_4) a_{\mathbf{k}_1 \sigma_1}^\dagger a_{\mathbf{k}_2 \sigma_2}^\dagger a_{\mathbf{k}_3 \sigma_2} a_{\mathbf{k}_4 \sigma_1} \\ & + \frac{1}{2} \sum_{\mathbf{k}_1 \mathbf{k}_2 \mathbf{k}_3 \mathbf{k}_4} \sum_{\sigma_1 \sigma_2} V_{\sigma_1 \sigma_2 \sigma_2 \sigma_1}^{vvvv}(\mathbf{k}_1 \mathbf{k}_2 \mathbf{k}_3 \mathbf{k}_4) b_{-\mathbf{k}_1, -\sigma_1}^\dagger b_{-\mathbf{k}_2, -\sigma_2}^\dagger b_{-\mathbf{k}_3, -\sigma_2} b_{-\mathbf{k}_4, -\sigma_1} \\ & - \sum_{\mathbf{k}_1 \mathbf{k}_2 \mathbf{k}_3 \mathbf{k}_4} \sum_{\sigma_1 \sigma_2} V_{\sigma_1 \sigma_2 \sigma_2 \sigma_1}^{cvvc}(\mathbf{k}_1 \mathbf{k}_2 \mathbf{k}_3 \mathbf{k}_4) a_{\mathbf{k}_1 \sigma_1}^\dagger b_{-\mathbf{k}_3, -\sigma_2}^\dagger b_{-\mathbf{k}_2, -\sigma_2} a_{\mathbf{k}_4 \sigma_1} \\ & - \sum_{\mathbf{k}_1 \mathbf{k}_2 \mathbf{k}_3 \mathbf{k}_4} \sum_{\sigma_1 \sigma_2 \sigma_3 \sigma_4} \bar{V}_{\sigma_1 \sigma_2 \sigma_3 \sigma_4}^{cvcv}(\mathbf{k}_1 \mathbf{k}_2 \mathbf{k}_3 \mathbf{k}_4) a_{\mathbf{k}_1 \sigma_1}^\dagger b_{-\mathbf{k}_4, -\sigma_4}^\dagger b_{-\mathbf{k}_2, -\sigma_2} a_{\mathbf{k}_3 \sigma_3}, \end{aligned} \quad (\text{B1})$$

where  $a_{\mathbf{k}\sigma}^\dagger$  ( $b_{\mathbf{k}\sigma}^\dagger$ ) is the creation operator for an electron (hole) with a wave function  $\psi_{\mathbf{k}\sigma}^{c(v)}$  of the Bloch form

$$\psi_{\mathbf{k}\sigma}^i(\mathbf{r}) = \frac{1}{\sqrt{\Omega}} u_{\mathbf{k}\sigma}^i(\mathbf{r}) \exp(i\mathbf{k} \cdot \mathbf{r}), \quad (\text{B2})$$

where  $\Omega$  is the normalization volume.  $E_c(\mathbf{k})$  and  $E_v(\mathbf{k})$  denote the band dispersions of the conduction and valence bands and the Coulomb matrix elements  $V$ 's are given by

$$V_{\sigma_1 \sigma_2 \sigma_3 \sigma_4}^{ijkl}(\mathbf{k}_1 \mathbf{k}_2 \mathbf{k}_3 \mathbf{k}_4) = \int d^3x d^3y \psi_{\mathbf{k}_1 \sigma_1}^{i*}(\mathbf{x}) \psi_{\mathbf{k}_2 \sigma_2}^{j*}(\mathbf{y}) v(|\mathbf{x}-\mathbf{y}|) \psi_{\mathbf{k}_3 \sigma_3}^k(\mathbf{y}) \psi_{\mathbf{k}_4 \sigma_4}^l(\mathbf{x}) \quad (\text{B3})$$

with  $v = e^2/(\epsilon|\mathbf{x}-\mathbf{y}|)$ .  $\bar{V}$  is given by the same expression as for  $V$  but with  $v$  replaced by  $e^2/|\mathbf{x}-\mathbf{y}|$ . The Hamiltonian (B1) is obtained from the many electron Hamiltonian by making a two-band approximation and keeping only those terms that conserve the number of the electron-hole pairs.<sup>54</sup> The effect of other excitations is phenomenologically included by screening the electron-hole Coulomb interaction. The electron-hole exchange interaction is, however, not screened.<sup>56</sup>

We consider cubic materials with a conduction band of  $\Gamma_6$  symmetry and a valence band of  $\Gamma_7$  symmetry, each two-fold degenerate. We note that the index  $\sigma = \pm 1/2$  in the expressions above refers to the spin in the case of the electron and to the  $j_z = \pm 1/2$  component of the  $\Gamma_7$  band in the case of the hole. For brevity, in what follows, we refer to this Bloch function angular momentum as ‘‘spin’’ in either case. The corresponding Bloch functions are of the form (at  $\mathbf{k}=0$ )

$$u_{0,1/2}^c(\mathbf{r}) = \zeta_0(\mathbf{r})\uparrow, \quad (\text{B4a})$$

$$u_{0,-1/2}^c(\mathbf{r}) = \zeta_0(\mathbf{r})\downarrow, \quad (\text{B4b})$$

$$u_{0,1/2}^v(\mathbf{r}) = \frac{-i}{\sqrt{3}}[\zeta_x(\mathbf{r}) + i\zeta_y(\mathbf{r})]\downarrow - \frac{i}{\sqrt{3}}\zeta_z(\mathbf{r})\uparrow, \quad (\text{B4c})$$

$$u_{0,-1/2}^v(\mathbf{r}) = \frac{-i}{\sqrt{3}}[\zeta_x(\mathbf{r}) - i\zeta_y(\mathbf{r})]\uparrow + \frac{i}{\sqrt{3}}\zeta_z(\mathbf{r})\downarrow, \quad (\text{B4d})$$

where  $\zeta_0$  is an  $s$ -like cell-periodic function and  $\zeta_x, \zeta_y, \zeta_z$  transform like  $x, y,$  and  $z$ .  $\uparrow$  and  $\downarrow$  denote the spin states.

A general electron-hole pair state may be constructed as

$$|p\rangle = \sum_{\mathbf{kk}'} C_{\mathbf{kk}'}^{I_z} |p_{\mathbf{kk}'}^{I_z}\rangle, \quad (\text{B5})$$

where  $|p_{\mathbf{kk}'}^{I_z}\rangle$  is the electron-hole pair state with total ‘‘spin’’  $I$  and its  $z$  component  $I_z$ :

$$|p_{\mathbf{kk}'}^{10}\rangle = \frac{1}{\sqrt{2}}(a_{\mathbf{k},1/2}^\dagger b_{\mathbf{k}',-1/2}^\dagger + a_{\mathbf{k},-1/2}^\dagger b_{\mathbf{k}',1/2}^\dagger)|0\rangle, \quad (\text{B6a})$$

$$|p_{\mathbf{kk}'}^{11}\rangle = a_{\mathbf{k},1/2}^\dagger b_{\mathbf{k}',1/2}^\dagger|0\rangle, \quad (\text{B6b})$$

$$|p_{\mathbf{kk}'}^{1,-1}\rangle = a_{\mathbf{k},-1/2}^\dagger b_{\mathbf{k}',-1/2}^\dagger|0\rangle, \quad (\text{B6c})$$

and

$$|p_{\mathbf{kk}'}^{00}\rangle = \frac{1}{\sqrt{2}}(a_{\mathbf{k},1/2}^\dagger b_{\mathbf{k}',-1/2}^\dagger - a_{\mathbf{k},-1/2}^\dagger b_{\mathbf{k}',1/2}^\dagger)|0\rangle. \quad (\text{B6d})$$

Minimization of the expectation value of  $H$  given by Eq. (B1) leads to

$$[E_c(\mathbf{k}) - E_v(\mathbf{k}) - E]C_{\mathbf{kk}'}^{I_z} - \sum_{\mathbf{ll}'} [V_{1/2,-1/2,-1/2,1/2}^{cvc}(\mathbf{k}, -\mathbf{l}', -\mathbf{k}', \mathbf{l}) - \delta_{l,1}\bar{V}_{1/2,-1/2,1/2,-1/2}^{cvc}(\mathbf{k}, -\mathbf{l}', \mathbf{l}, -\mathbf{k}')]C_{\mathbf{ll}'}^{I_z} = 0. \quad (\text{B7})$$

Now we make the effective mass approximation for the band dispersions and evaluate the Coulomb matrix elements in the Wannier approximation:<sup>54</sup>

$$V_{1/2,-1/2,-1/2,1/2}^{cvc}(\mathbf{k}, -\mathbf{l}', -\mathbf{k}', \mathbf{l}) = \frac{1}{\Omega^2} \int d^3x d^3y \exp[i(\mathbf{l}-\mathbf{k})\cdot\mathbf{x} + i(\mathbf{l}'-\mathbf{k}')\cdot\mathbf{y}] v(|\mathbf{x}-\mathbf{y}|), \quad (\text{B8a})$$

$$\bar{V}_{1/2,-1/2,1/2,-1/2}^{cvc}(\mathbf{k}, -\mathbf{l}', \mathbf{l}, -\mathbf{k}') = \pi a_{\text{ex}}^3 \Delta E_{\text{exch}}^0 \frac{1}{\Omega^2} \int d^3x \exp[i(\mathbf{l}-\mathbf{k}+\mathbf{l}'-\mathbf{k}')\cdot\mathbf{x}] \quad (\text{B8b})$$

with

$$\pi a_{\text{ex}}^3 \Delta E_{\text{exch}}^0 = \frac{2}{3\Omega_{\text{cell}}} \int d^3x d^3y \frac{e^2}{|\mathbf{x}-\mathbf{y}|} \zeta_0(\mathbf{x})\zeta_x(\mathbf{y})\zeta_0(\mathbf{y})\zeta_x(\mathbf{x}), \quad (\text{B8c})$$

where  $\Omega_{\text{cell}}$  is the volume of a unit cell.<sup>57</sup>  $\Delta E_{\text{exch}}^0$  equals the bulk exciton exchange splitting, within the present approximation. Invoking the above approximations on Eq. (B7), and Fourier transforming to the real space, we get Eq. (9) of Sec. II. We note that  $I$  is not the real spin but stands for the sum of the Bloch function angular momenta of the electron and the hole. Using the hydrogenic wave function of the bulk exciton, it is easy to verify that  $\Delta E_{\text{exch}}^0$  equals the bulk exciton exchange splitting energy.

Now we derive the biexciton EMA equation [Eq. (13)]. For the total ‘‘spin’’  $J=0$ , a general two-pair state may be written as

$$|m\rangle = \sum_{\mathbf{kk}'\mathbf{ll}'} \sum_{S=0,1} K_{\mathbf{kk}'\mathbf{ll}'}^{SS} |m_{\mathbf{kk}'\mathbf{ll}'}^{SS}\rangle \quad (\text{B9a})$$

with

$$|m_{\mathbf{k}\mathbf{k}'\mathbf{l}\mathbf{l}'}^{00}\rangle = \frac{1}{4} \sum_{\sigma_1, \sigma_2} (-1)^{(\sigma_1 - \sigma_2)} a_{\mathbf{k}, \sigma_1}^\dagger a_{\mathbf{k}', -\sigma_1}^\dagger b_{\mathbf{l}, \sigma_2}^\dagger b_{\mathbf{l}', -\sigma_2}^\dagger |0\rangle, \quad (\text{B9b})$$

and

$$|m_{\mathbf{k}\mathbf{k}'\mathbf{l}\mathbf{l}'}^{11}\rangle = \frac{1}{2\sqrt{3}} \left[ \sum_{\sigma} a_{\mathbf{k}, \sigma}^\dagger a_{\mathbf{k}', \sigma}^\dagger b_{\mathbf{l}, -\sigma}^\dagger b_{\mathbf{l}', -\sigma}^\dagger - \frac{1}{2} \sum_{\sigma_1, \sigma_2} a_{\mathbf{k}, \sigma_1}^\dagger a_{\mathbf{k}', -\sigma_1}^\dagger b_{\mathbf{l}, \sigma_2}^\dagger b_{\mathbf{l}', -\sigma_2}^\dagger \right] |0\rangle. \quad (\text{B9c})$$

The antisymmetry of the wave function under the electron-electron (hole-hole) exchange requires that  $K^{00}$  be even and  $K^{11}$  be odd under the interchange of  $\mathbf{k}, \mathbf{k}'$  or  $\mathbf{l}, \mathbf{l}'$ . Proceeding as in the case of the exciton, we get Eq. (13).

To derive the EMA equations for  $J=1$  and  $J=2$  biexciton states, we note that a general two-pair state with total ‘‘spin’’  $J$  and its  $z$  component  $J_z$  may be written as

$$|m\rangle_{JJ_z} = \sum_{\mathbf{k}\mathbf{k}'\mathbf{l}\mathbf{l}'} \sum_{S, S'=0,1} K_{\mathbf{k}\mathbf{k}'\mathbf{l}\mathbf{l}'}^{SS'} |m_{\mathbf{k}\mathbf{k}'\mathbf{l}\mathbf{l}'}^{SS'}(JJ_z)\rangle \quad (\text{B10})$$

with

$$|m_{\mathbf{k}\mathbf{k}'\mathbf{l}\mathbf{l}'}^{SS'}(JJ_z)\rangle = \frac{1}{2} \sum_{ss'=\pm 1/2} \sum_{\sigma_1, \sigma_1'=\pm 1/2} \sum_{\sigma_2, \sigma_2'=\pm 1/2} C_{ss'M}^{SS'J} C_{\sigma_1 \sigma_1' s}^{1/2 1/2 S} C_{\sigma_2 \sigma_2' s'}^{1/2 1/2 S'} a_{\mathbf{k}, \sigma_1}^\dagger a_{\mathbf{k}', \sigma_1'}^\dagger b_{\mathbf{l}, \sigma_2}^\dagger b_{\mathbf{l}', \sigma_2'}^\dagger |0\rangle, \quad (\text{B11})$$

where the  $C$ 's denote the Clebsch-Gordan coefficients. The EMA equations (15) and (17) for  $J=1$  and  $J=2$  states may now be derived as for the case for  $J=0$ .

\*On leave from the Centre for Advanced Technology, Indore 452013, India.

<sup>1</sup> *Microcrystalline and Nanocrystalline Semiconductors*, edited by R. W. Collins, C. C. Tsai, M. Hirose, F. Koch, and L. Brus, MRS Symposia Proceedings No. 358 (Materials Research Society, Pittsburgh, 1995).

<sup>2</sup> S. Schmitt-Rink, D. A. B. Miller, and D. S. Chemla, *Phys. Rev. B* **35**, 8113 (1987).

<sup>3</sup> T. Takagahara, *Phys. Rev. B* **39**, 10 206 (1989).

<sup>4</sup> E. Hanamura, *Phys. Rev. B* **37**, 1273 (1988).

<sup>5</sup> S. V. Nair and K. C. Rustagi, *Superlatt. Microstruct.* **6**, 337 (1989).

<sup>6</sup> R. K. Jain and R. C. Lind, *J. Opt. Soc. Am.* **73**, 647 (1983).

<sup>7</sup> P. Roussignol, D. Ricard, and C. Flytzanis, *Appl. Phys. A* **44**, 285 (1987).

<sup>8</sup> J. Yumoto, S. Fukushima, and K. Kubodera, *Opt. Lett.* **12**, 832 (1987).

<sup>9</sup> Y. Masumoto, T. Kawamura, and K. Era, *Appl. Phys. Lett.* **62**, 225 (1993).

<sup>10</sup> T. Kataoka, T. Tokizaki, and A. Nakamura, *Phys. Rev. B* **48**, 2815 (1993).

<sup>11</sup> V. Colvin, M. Schlamp, and A. P. Alivisatos, *Nature (London)* **370**, 354 (1994).

<sup>12</sup> B. O. Dabbousi, M. G. Bawendi, O. Onitsuka, and M. F. Rubner, *Appl. Phys. Lett.* **66**, 1316 (1995).

<sup>13</sup> A. L. Efros and A. L. Efros, *Phys. Tekh. Poluprovodn.* **16**, 1209 (1982) [*Sov. Phys. Semicond.* **16**, 772 (1982)].

<sup>14</sup> A. Nakamura, H. Yamada, and T. Tokizaki, *Phys. Rev. B* **40**, 8585 (1989).

<sup>15</sup> T. Itoh, T. Ikehara, and Y. Iwabuchi, *J. Lumin.* **45**, 29 (1990); T. Itoh, M. Furumiya, and T. Ikehara, *Solid State Commun.* **73**, 271 (1990).

<sup>16</sup> E. Hanamura, *Solid State Commun.* **62**, 465 (1987).

<sup>17</sup> K. Edamatsu, S. Iwai, T. Itoh, S. Yano, and T. Goto, *Phys. Rev. B* **51**, 11 205 (1995).

<sup>18</sup> P. E. Lippens and M. Lannoo, *Phys. Rev. B* **39**, 10 935 (1989).

<sup>19</sup> L. M. Ramaniah and S. V. Nair, *Phys. Rev. B* **47**, 7132 (1993).

<sup>20</sup> A. I. Ekimov, F. Hache, M. C. Schanne-Klein, D. Ricard, C.

Flytzanis, I. A. Kudryavtsev, T. V. Yazeva, A. V. Rodina, and A. L. Efros, *J. Opt. Soc. Am. B* **10**, 100 (1993).

<sup>21</sup> L.-W. Wang and A. Zunger, *J. Chem. Phys.* **100**, 2394 (1994).

<sup>22</sup> L.-W. Wang and A. Zunger, *Phys. Rev. B* **53**, 9579 (1996).

<sup>23</sup> Y. Kayanuma, *Solid State Commun.* **59**, 405 (1986).

<sup>24</sup> S. V. Nair, S. Sinha, and K. C. Rustagi, *Phys. Rev. B* **35**, 4098 (1987).

<sup>25</sup> T. Takagahara, *Phys. Rev. B* **36**, 9293 (1987).

<sup>26</sup> Y. Kayanuma, *Phys. Rev. B* **38**, 9797 (1988).

<sup>27</sup> T. Takagahara, *Phys. Rev. B* **47**, 4569 (1993).

<sup>28</sup> Y. Z. Hu, M. Lindberg, and S. W. Koch, *Phys. Rev. B* **42**, 1713 (1990).

<sup>29</sup> L. Belleguie and L. Bányai, *Phys. Rev. B* **44**, 8785 (1991).

<sup>30</sup> S. V. Nair and T. Takagahara, *Phys. Rev. B* **53**, R10 516 (1996).

<sup>31</sup> K. Cho, in *Excitons*, edited by K. Cho (Springer, Berlin, 1979), and references therein.

<sup>32</sup> G. F. Koster, J. O. Dimmock, R. G. Wheeler, and H. Statz, *Properties of Thirty-Two Point Groups* (MIT Press, Cambridge, MA, 1963).

<sup>33</sup> K. Edamatsu, Y. Mimura, K. Yamanaka, and T. Itoh (unpublished).

<sup>34</sup> T. Itoh and K. Edamatsu (unpublished).

<sup>35</sup> M. Ueta, H. Kanzaki, K. Kobayashi, Y. Toyozawa, and E. Hanamura, *Excitonic Processes in Solids* (Springer, Berlin, 1986).

<sup>36</sup> O. Akimoto and E. Hanamura, *Solid State Commun.* **10**, 253 (1972).

<sup>37</sup> W. F. Brinkman, T. M. Rice, and B. Bell, *Phys. Rev. B* **8**, 1570 (1973).

<sup>38</sup> F. Bassani, J. J. Forney, and A. Quattropani, *Phys. Status Solidi B* **65**, 591 (1974).

<sup>39</sup> N. Nagasawa (private communication).

<sup>40</sup> Y. Masumoto, S. Okamoto, and S. Katayanagi, *Phys. Rev. B* **50**, 18 658 (1994).

<sup>41</sup> *Physics of II-VI and I-VII Compounds, Semimagnetic Semiconductors*, edited by O. Madelung, M. Schulz, and H. Weiss, Landolt-Börnstein, New Series, Group III, Vol. 17, Pt. b (Springer, Berlin, 1982). We obtain the exciton Rydberg by add-

- ing 4.4 meV of exchange energy to the binding energy of the  $\Gamma_5$  exciton quoted here.
- <sup>42</sup>T. Itoh, Y. Iwabuchi, and M. Kataoka, *Phys. Status Solidi B* **145**, 567 (1988).
- <sup>43</sup>R. Shimano and M. Kuwata-Gonokami, *Phys. Rev. Lett.* **72**, 530 (1994).
- <sup>44</sup>H. Akiyama, T. Kuga, M. Matsuoka, and M. Kuwata-Gonokami, *Phys. Rev. B* **42**, 5261 (1990).
- <sup>45</sup>M. Ikezawa and Y. Masumoto, *Phys. Rev. B* **53**, 13 694 (1996).
- <sup>46</sup>C. Flytzanis, in *Quantum Electronics: A Treatise*, edited by H. Rabin and C. L. Tang (Academic, New York, 1975), Vol. I. Also, see, Eq. (6.1) of Ref. 3.
- <sup>47</sup>These two terms arise from the first term in Eq. (31) which, in the present case, dominates over the second term because  $\gamma_{\parallel}^e \ll \gamma_{eg}$ .
- <sup>48</sup>D. W. Hall and N. F. Borrelli, *J. Opt. Soc. Am. B* **5**, 1650 (1988); S. H. Park, R. A. Morgan, Y. Z. Hu, M. Lindberg, S. W. Koch, and N. Peyghambarian, *ibid.* **7**, 2097 (1990); P. Roussignol, D. Ricard, and C. Flytzanis, *Appl. Phys. B* **51**, 437 (1990); H. Shinojima, J. Yumoto, and N. Uesugi, *Appl. Phys. Lett.* **60**, 298 (1992); M. C. Schanne-Klein, F. Hache, D. Ricard, and C. Flytzanis, *J. Opt. Soc. Am. B* **9**, 2234 (1992).
- <sup>49</sup>M. C. Schanne-Klein, L. Piveteau, M. Ghanassi, and D. Ricard, *Appl. Phys. Lett.* **67**, 579 (1995).
- <sup>50</sup>M. G. Bawendi, W. L. Wilson, L. Rothberg, P. J. Carroll, T. M. Jedju, M. L. Steigerwald, and L. E. Brus, *Phys. Rev. Lett.* **65**, 1623 (1990).
- <sup>51</sup>D. J. Norris, A. Sacra, C. B. Murray, and M. G. Bawendi, *Phys. Rev. Lett.* **72**, 216 (1994).
- <sup>52</sup>Y. Masumoto (private communication).
- <sup>53</sup>L. Belleguie and L. Bányai, *Phys. Rev. B* **47**, 4998 (1993).
- <sup>54</sup>E. Hanamura and H. Haug, *Phys. Rep.* **33C**, 209 (1977).
- <sup>55</sup>This equation is the same as Eq. (2.7) of Ref. 54 except that we explicitly take into account the spin-orbit coupled nature of the valence band.
- <sup>56</sup>L. J. Sham and T. M. Rice, *Phys. Rev.* **144**, 708 (1966).
- <sup>57</sup>We have neglected the long range part of the exchange interaction which is expected to be small (see Ref. 27).